Impact of CO$_2$ hydrates on injectivity during CO$_2$ storage in depleted gas fields
A literature review

Aghajanloo, Mahnaz; Yan, Lifei; Berg, Steffen; Voskov, Denis; Farajzadeh, Rouhi

Important note
To cite this publication, please use the final published version (if applicable).
Please check the document version above.

Impact of CO$_2$ hydrates on injectivity during CO$_2$ storage in depleted gas fields: A literature review

Mahnaz Aghajanloo [a,*], Lifei Yan [a], Steffen Berg [b], Denis Voskov [a,c], Rouhi Farajzadeh [a,b]

[a] *Delft University of Technology, Department of Geoscience and Engineering, Stevinweg 1, 2628 CN, Delft, the Netherlands*
[b] *Shell Global Solutions International B.V., Grasweg 31, 1031 HW, Amsterdam, the Netherlands*
[c] *Energy, Science and Engineering, Stanford University, USA*

ARTICLE INFO

ABSTRACT

Carbon dioxide capture and storage in subsurface geological formations is a potential solution to limit anthropogenic CO$_2$ emissions and combat global warming. Depleted gas fields offer significant CO$_2$ storage volumes; however, injection of CO$_2$ into these reservoirs poses some potential challenges for the injectivity, containment and well/facility integrity due to low temperatures caused by isenthalpic expansion of CO$_2$. A key injectivity risk is due to possible formation of hydrates at the low expected temperatures. This study aims to address main causes of CO$_2$ hydrate formation and its impact on permeability of porous media. This review highlights the current state of knowledge in the literature while emphasizing the need to bridge existing gaps in derisking CO$_2$ injection into (depleted) low-pressure gas reservoirs. In summary, according to the existing literature, the potential for hydrate formation is assessed to be credible. Current industry solutions exist to manage this risk; however, they are costly and energy intensive. Future research will be needed to provide capabilities to manage this risk more efficiently.

1. Introduction

According to the newest report from the Intergovernmental Panel on Climate Change (IPCC), carbon dioxide (CO$_2$), the predominant greenhouse gas released from anthropogenic activities, contributed to 80% of the total greenhouse gas emissions (Levin et al., 2022; Parmesan et al., 2022). Recent research indicates that Carbon Capture and Storage (CCS) technologies offer an effective approach to mitigating the adverse effects resulting from excessive CO$_2$ emissions (Davoodi et al., 2023). Among various geological formations, CO$_2$ storage in depleted gas fields has significant benefits compared to other subsurface storage options such as aquifers and depleted oil fields (Pan et al., 2021; Peter et al., 2022; Tamáskovics et al., 2023). The risks and uncertainties associated with the deplete gas fields are comparatively lower because of their extended production history, proven sealing capacity, and (partial) availability of infrastructure and equipment required to store CO$_2$. However, injection of CO$_2$ into these reservoirs poses some potential challenges for CO$_2$ injectivity, containment and well/facility integrity due to low temperatures caused by various thermodynamic phenomena including isenthalpic expansion of CO$_2$ (Chesnokov et al., 2023). The conventional solution to this issue is to heat CO$_2$ at the surface and insulate injection

stream before injection; however, this comes at a high cost given the short duration of the risk exposure and is CO$_2$ intensive resulting in reduced net CO$_2$ storage capacity.,

The success of these projects largely depends on the injectivity of the well, which is critical to reach injection targets to limit greenhouse-gas related temperature increase, the achievement of which is in practice imposed by contractual or regulatory commitments. Injectivity is defined as the mass or volume of injected CO$_2$ for a certain pressure gradient (Hoteit et al., 2019; Yusof et al., 2022). Permeability can be impaired during the CO$_2$ injection for a number of reasons both in hydrocarbon recovery (Farajzadeh et al., 2019; Ikeda et al.; Ochi and Vernoux, 1998; Valadbeygian et al., 2023) and CO$_2$ sequestration (Sokama-Neuyam et al., 2023; Xie et al., 2017), operations. There are a number of possible countermeasures, which typically have either technical or economic limitations. For instance, to maintain the flowrate the well pressure should increase. However, beyond a certain (fracture) pressure, the reservoir rock will break, which poses a serious containment risk and is typically not permissible. Therefore, either the CO$_2$ injection rate should be reduced, which would compromise sequestration targets, or the injectivity should be restored by remedial action.

Several factors or mechanisms can lead to impairment of injectivity

---

of CO_2 wells. Injectivity impairment might be caused, for example, by the evaporation of water into dry or undersaturated CO_2 which can lead to the precipitation of salt (mainly halite) and thus plugging of the reservoir pores (Ott et al., 2021).

For CCS in low-pressure or depleted reservoirs, thermodynamic properties of CO_2 play a major role. CO_2 is usually transported to site location in liquid or supercritical state and injection is conducted in the state of high mass density to achieve sequestration targets (Shotton et al., 2022). The injection of high-pressure CO_2 into low pressure reservoirs leads to isenthalpic expansion of CO_2 which then causes a decrease in temperature (Chesnokov et al., 2023; Loeve et al., 2014). The magnitude of the temperature reduction depends on CO_2 flowrate, reservoir permeability, thickness and thermal properties of the rock and the in-situ brine, and well radius and completion (Mathias et al., 2010). For typical CO_2 injection rates (~1Mtpa), the temperature is expected to be very low (Almenningen et al., 2021). If the temperature is below the hydrate phase boundary inside stability zone (see Fig. 1) and enough water is available in the porous medium, solid hydrates can form, which can reduce the porosity and eventually the permeability.

While hydrate formation has always played an important role in production, transportation and processing of hydrocarbons e.g. in pipelines (Sayani et al., 2020), and also methane hydrates at continental slopes are considered as a potential source of hydrocarbons (Demirbas, 2010; Englezos and Lee, 2005), there is a concrete case of relevance of CO_2 hydrates when CO_2 sequestration (CCS) in depleted gas fields is considered (Bui et al., 2018). Hydrate formation is considered as one of the major potential risks for the implementation of CO_2 storage in ultra-depleted reservoirs (<50 bar) (Sloan and Fleyfel, 1991). Formation of hydrates in porous media, apart from pressure and temperature, is influenced by several parameters related to properties of the rock (permeability, porosity, mineralogy), water (saturation, composition, salinity, type of salt) and gas (type, composition, or purity). To quantify and/or to design strategies to prevent or mitigate the impact of CO_2 hydrate on the injectivity, it is necessary to understand the impact of different factors on hydrate formation in porous media.

Over the past decades, much research has been conducted on CO_2 hydrate inside the bulk under various conditions and materials (Yang et al., 2013; Zheng et al., 2020). However, to the best of our knowledge,

no review has been done on CO_2 hydrate formation/elimination in the context of CCS projects, especially on the topic of CO_2 injectivity in depleted gas fields. There are only a few precedence cases from the literature for CO_2 hydrate formation at field scale or field-related processes or projects. Most field examples (Gauteplass et al., 2020b; Jadhawar et al., 2006) are scattered and not at conditions relevant for CO_2 injection in depleted gas fields. Nevertheless, these examples demonstrate that in principle CO_2 hydrates or ice can form (Li et al., 2023; Semenov et al., 2023) and, if hydrates or ice formed (by different processes) (Sloan and Fleyfel, 1991; Zhang and Guo, 2017), they can significantly impair injectivity. However, there is no demonstrated case where CO_2 hydrates form due to the isenthalpic expansion cooling effect during CO_2 injection. In a field containing mainly CO_2, solids were formed which were identified as hydrates and/or ice (Xu et al., 2007); this demonstrates that hydrates or ice can indeed form in the field. Notice that in these cases, the solids were observed during production downstream of the separator and not during injection into the porous medium. Provision had been made for methanol injection to suppress hydrates, but this proved ineffective. In a water-alternating gas (WAG) pilot, hydrocarbon gas was injected, and due to expansion of the hydrocarbon gases the temperature dropped, and hydrates formed. Consequently, gas injection rates dropped to zero in a matter of hours (Jensen et al., 2000). However, in this example, gas was injected in a well that had injected water for an extended period (44 million barrels). Consequently, the temperature in the near wellbore had dropped to 285K from the initial 403K (12 °C, 130 °C) at a reservoir depth of approximately 3000 m. This occurred in an area where the surrounding seawater temperatures are low, and the pressure is about 300 bar (Adeniyi and Ezeagu, 2020). These conditions fall within the hydrate window for hydrocarbon gas. Note that these are different conditions than the injection of CO_2 in depleted gas fields. The low temperature was most likely not due to isenthalpic expansion but to prolonged cold sea water injection.

Besides the above-mentioned cases, an injectivity impairment was demonstrated in an integrated experiment where the cooling effects from injection led to a complete blockage (Maloney and Briceno, 2009). All these examples show that the formation of hydrates in an injection scenario is not just hypothetical. There are concrete precedent cases of hydrate formation in the near-well region due to gas injection, although the conditions and chemical composition of reservoir fluids varied and none of them were close to the conditions expected for CO_2 injection in ultra-depleted gas fields.

The aim of this review is to provide an overview of the conditions and factors that facilitate or hinder the potential of large-scale CCS in depleted gas fields to support the assessment of the overall risk of hydrate formation for CCS in depleted gas reservoirs. Besides a set of actions that can be affordable and implemented to reduce the risk of CO_2 hydrate formation during injection will be assessed. It will be demonstrated that the kinetics of hydrate formation and propagation in porous media exhibit distinct behavior compared to a bulk environment. The properties of porous media, e.g., heterogeneous permeability, wettability, residual water saturation, gas impurity, and brine salinity, have varying degrees of impact on the hydrate formation and dissociation, which will be reviewed. The intrinsic factors of gas hydrate, e.g., memory effect (Rossi et al., 2021; Wen et al., 2021) and self-preservation effect (Vlasov, 2019) have a significant influence on the kinetic behavior of hydrate. Since, those factors compose a complicated system for tackling hydrate issues in the depleted gas field, their impact on CO_2 hydrate formation/dissociation process and its feasibility will be discussed. Furthermore, the likely simultaneous phenomenon of salt dry-out and gas hydrate is theoretically argued for the CO_2 injection. The interactions between the injection well and reservoir will be described for the corresponding thermodynamic conditions during hydrate formation and dissociation. Following that, feasible prevention approaches will be reviewed. Finally, we will discuss the scientific and engineering problems facing hydrate formation in porous reservoirs,

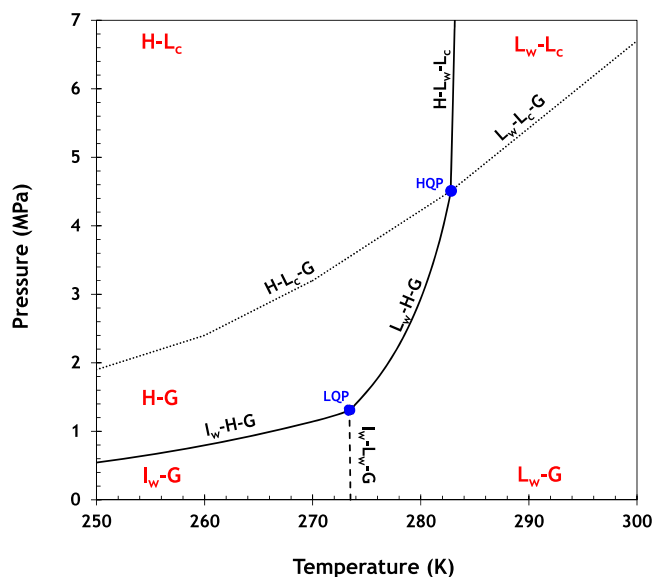**Fig. 1.** Three-phase diagram of the CO_2-water mixture. The symbols I_w, L_c, L_w, H, and G represent ice water, liquid CO_2, liquid water, hydrate, and gas, respectively. HQP and LQP refer to high (L_wHL_CG) and low (I_wHL_WG) quadruple points. The smooth line represent the three-phase equilibrium line, the dotted line indicate the CO_2 condensed line, and the dashed line is ice line.

based on our current limited understanding.

2. Gas hydrate types and structure

Gas hydrates or clathrate hydrates are ice-like crystalline compounds composed of a low molecular weight gas (usually light hydrocarbons and water-soluble gases) and water molecules, combined under certain thermodynamic conditions (relatively high pressure and low temperature). In a clathrate hydrate network, water as a host forms a cage-like lattice structure through H-bonding surrounding the guest gas molecules (Sloan, 2003). Depending on the size and purity of the guest gas molecules, the number of water molecules participating in lattice clusters varies and determines the type of hydrate structure (Cai et al., 2022). In general, guest gas molecules have an important function in the stability of the hydrate structures in which the water molecules form a cage around the guest molecules. Because the structure of the clathrate hydrates is not based on covalent bonds but rather a hydrogen bonded framework, the process of their formation and dissociation is a first-order phase transition rather than chemical reactions (Sloan and Koh, 2008). The exothermic process of hydrate formation could be characterized by two steps: (1) the nucleation step, which is the conversion from an unstable condition to stable growth (until critical particle size is reached), and (2) the growth step. Hydrate nucleation can occur in several ways. Because the transport of the gas and water molecules across the hydrate layers is limited, the growth step can be slow. In general, the hydrate formation starts with dissolution of the gas molecules in the aqueous phase followed by producing labile unstable clusters (Sloan and Fleyfel, 1991). Hydrate nucleation is determined as an activated microscopic phenomenon in which many molecules agglomerate and create individual clusters that subsequently transform into hydrate nuclei. When these small nuclei reach a critical size, consecutive growth begins (Lederhos et al., 1996).

The known hydrate structures are classified into three main types: the cubic structures I (sI) and II (sII) and the hexagonal structure H (sH), as schematically shown in Fig. 2. All structures consist of five different host water cages and are approximately 85% water and 15% gas on a molar basis when all the cages are occupied (Martinez et al., 2022). Structure I, which is the most common gas hydrate structure, includes two small pentagonal dodecahedra (5^{12}) and six tetrakaidecahedra ($5^{12}6^2$) per unit cell. Hydrate sI is the simplest structure with an average lattice structure of 12.1 Å, which holds small gas molecules (0.4–0.55 nm) in a unit cell of 46 water molecules. Clathrate hydrate structure sII is a 17.2 Å cube composed of 136 water molecules of 16 pentagonal dodecahedrons (5^{12}) followed by 8 hexakaidecahedrons ($5^{12}6^4$) and trapping larger gas molecules (0.6–0.7 nm). Structure H is the only structure consisting of three cavities with the combination of three pentagonal dodecahedrons (5^{12}), two irregular dodecahedrons ($4^35^66^3$), and one icosahedron ($5^{12}6^8$), with an average lattice structure between 12.2 Å to 10.1 Å. The sH hydrate structure requires concomitantly small gas molecules (as auxiliary gas) such as those forming sI and larger molecule typically liquid hydrocarbons (0.75–0.9 nm).

In general, CO_2 forms the most common hydrate structure sI in the presence of free water under certain thermodynamic conditions depicted in Fig. 1 (Wroblewski, 1882). In Structure I, the hydrate nuclei are formed by connecting the large cages with pentagonal or hexagonal faces to the small cages. By joining these hydrate nuclei to each other, hydrate clusters are formed and adsorb the CO_2 molecule from the water phase to their surface. The upper part of the interconnected surfaces of the two cages is the favorable adsorption site for CO_2 molecules and can prepare two common pentagonal faces for further CO_2 hydrate formation. Next, the water molecules gradually and continually form cages around the CO_2 molecules and encage the CO_2 molecules into the clathrate structure. Theoretical and experimental evidence also supports the existence of metastable structures sII (Cabrera-Ramírez and Prosmiti, 2022; Fleyfel and Devlin, 1991; Lee et al., 2023; Staykova et al., 2003) and sH (Alavi and Woo, 2007; Cabrera-Ramírez and Prosmiti, 2022) of CO_2 hydrates under thermodynamic conditions approaching the ice melting point. Moreover, there is confirmation regarding the formation of CO_2 hydrate semi-clathrates with other guest components (Kumar et al., 2009; Torré et al., 2012; Zheng et al., 2017).

The following equation can be written for CO_2 hydrate formation/dissociation process (Nagashima et al., 2020):
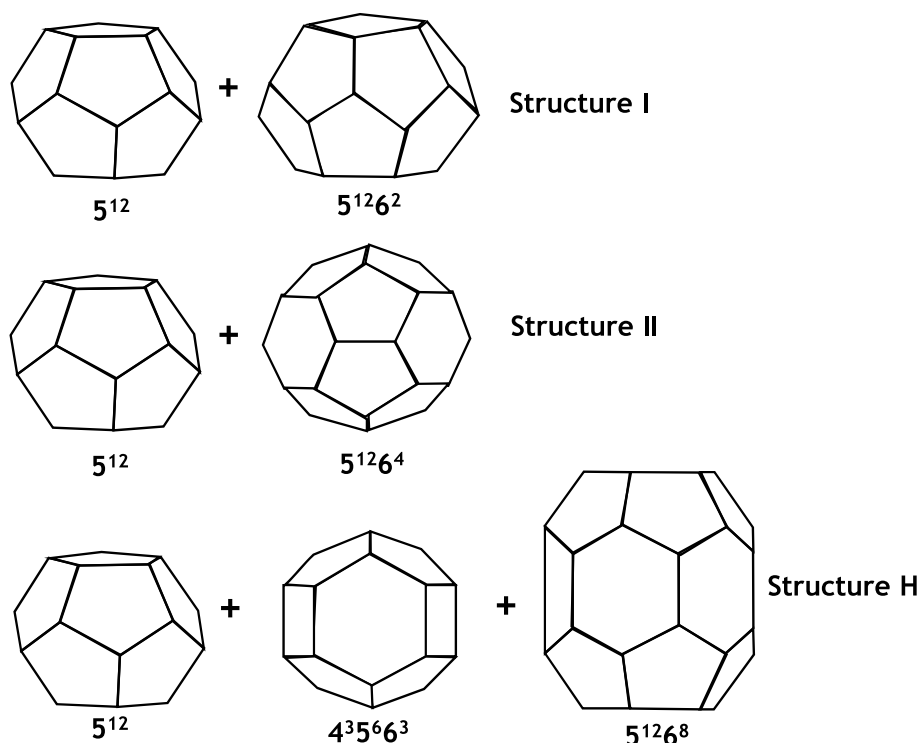

Fig. 2. Three common hydrate unit crystal structures, Adopted from (Gaidukova et al., 2022; Koh et al., 2011; Sloan, 2003).

$$CO_2 + n_h H_2O \leftrightarrow CO_2 \cdot n_h H_2O + \Delta H \qquad (1)$$

where n_h is the hydration number or the number of water molecules per guest gas molecule. ΔH represents the enthalpy of formation/dissociation of hydrate (exothermic heat released or endothermic heat absorbed) during phase transition, which causes the difference in the slope between I_w-H-G and L_w-H-G lines (see Fig. 1). Formation of gas hydrate is closely linked to the hydration number. In the case of CO_2 hydrate, which is mainly in the form of structure sI, the theoretical hydration number is approximately 5.75. However, achieving this value requires full occupancy of both small and large cavities.

3. Hydrate formation in porous media

In this section, we will review various aspects of affecting hydrate formation in porous media due to injection of CO_2. Formation and dissociation of CO_2 hydrate under bulk conditions (i.e., two-phase conditions in the absence of solid substrates) have been studied by many researchers (Dholabhai et al., 1993). The CO_2 concentration (CO_2 flow introduced into the bulk) in the bulk condition has a considerable impact on the properties of CO_2 hydrate formation and dissociation (Han et al., 2010). In the absence of flow, when the amount of CO_2 is inadequate to completely saturate the aqueous phase, pressure decreases considerably outside the hydrate stability zone and prevents the crystallization or breaking of the fragile hydrate crystals in their primary stages. In contrast, for high CO_2 concentrations, the aqueous phase is entirely saturated by CO_2 molecules and as a result, nucleation and crystallization of CO_2 hydrate take place (Hosseini Zadeh et al., 2021; Khurana et al., 2017). In addition, as the volumetric ratio of CO_2 increases, the time of decomposition and equilibration becomes longer and leads to creation of dense and relatively stable hydrate. Generally, hydrate formation in a bulk condition is influenced by the gas concentration, the gas–water interfacial area, mass transfer rate, and gas solubility in the aqueous phase, in addition to temperature and pressure conditions.

3.1. Impact of porous media on hydrate formation

There is a significant difference between formation of hydrate in the bulk fluids and within porous media (Wang et al., 2022). The nucleation mechanisms involve interfaces, either gas-liquid (hydrates form at the interface between connate water and gas) or liquid-solid (hydrates in super-saturated brine form at the solid surface, mainly at clay minerals), which are significantly different in porous media than in bulk fluid experiments (Kvamme et al., 2020; Zhang et al., 2021).

Due to the exothermic nature of the hydrate formation, the nucleation and subsequent growth typically lead to an increase in the bulk temperature and a change in the bulk density of the phases (Yin et al., 2021). On the contrary, due to faster heat transfer in the porous medium, hydrate nucleation and growth do not have a noticeable effect on the pressure and temperature change inside porous medium (Zhang et al., 2021). Characteristics of porous media such as permeability (Xu et al., 2022), porosity, wettability (Li et al., 2022), mineral composition, pore size distribution (PSD)(Chong et al., 2016; Zhang et al., 2021), roughness, and water saturation (Benmesbah et al., 2020; Jasamai et al., 2016) have a decisive role on hydrate nucleation and growth (crystallization). A porous medium has a vast specific surface area that can lead to increase of the gas−water interface. Furthermore, the solid surface provides large area for water molecules to organize and promote nucleation sites (Yang et al., 2010; Zatsepina and Buffett, 2002). Nevertheless, when the pore sizes are too large, the thermodynamic conditions of hydrate formation are similar to the bulk conditions. This is because the gas molecules are present in the micro pores, where water molecules have minimum activity (Liu et al., 2022; Wang et al., 2022; Zhang et al., 2018). However, the inhibition impact of meso- and macro pores is relatively weaker (2 nm < meso<50 nm < macro) ("Chapter 2 -

Structural Control of Nanoparticles," 2018). Therefore, as the pore size decreases, the risk of hydrate formation becomes lower (the hydrate phase boundary shown in Fig. 1 displaces to the left). This is attributed to the reduction of water activity in the porous medium owing to the dominant impact of capillary forces (Wu et al., 2021). Furthermore, the temperature of hydrate dissociation in porous media is lower than the decomposition temperatures in bulk due to existence of the capillary force (Geng et al., 2021; Nair et al., 2016). This indicates that hydrate formation is usually not a thermodynamically equilibrium step (it may not be repeatable) and depend on several factors, including agitation/turbulency, cooling rate, presence of additives, fluid composition, water memory, and degree of subcooling (Gambelli et al., 2022). Inside individual pores of porous media, hydrates can assume several different morphologies, which are sketched in Fig. 3. Pore filling hydrates nucleate within pore spaces or along grain surfaces without bridging grain particles. Contact cementing hydrates nucleate at the contact points between grains, serving as a cement, and grow around these points. Patchy hydrates nucleate and grow within pore spaces. Grain-coating hydrates nucleate on grain surfaces and coats their surface. Load-bearing hydrates nucleate in pores or grain surfaces, growing towards adjacent sands, while supporting matrix hydrates grow between grains, integrating into the sediment framework.

Furthermore, the presence of the porous medium significantly affects the bulk properties in addition to influencing the hydrate morphology at the pore level. This is because, apart from nucleation at the pore level, the growth requires capillary-driven transport, which limits the mass transfer (Handa and Ohsumi, 1995). One of the practical consequences is that CO_2 hydrates may preferentially form outside of the porous medium than inside (Ballard et al., 2001); however, this statement cannot be generalized because clay minerals have also been observed to act as nucleation seeds for hydrate formation.

3.1.1. Kinetics of CO_2 hydrate in porous media

The kinetics of CO_2 hydrate formation and dissociation plays an important role is assessing the injectivity of CO_2 injection wells. The regions with faster growth rates can lead to more severe hydrate plugging of the pores, potentially affecting the injectivity of CO_2 into the reservoir. Similarly, the rate of hydrate dissociation determines how fast or slow the injectivity of the wells are retrieved.

The nucleation of hydrates is a stochastic process that involves a substantial delay period lasting from hours to days, particularly in the absence of promoting agents. (Bai et al., 2015; Ke et al., 2019). To accurately determine the nucleation process and growth pattern induction times, numerous individual experiments are required to gather relevant statistical data. (Talaghat and Khodaverdilo, 2019). This is important when conducting laboratory experiments which need to be designed to last for several hours to reach a nucleation probability of 1 to provide reliable evidence for or against the occurrence of hydrates. Experiments that last only few minutes may miss the nucleation of hydrates. Also, in experiments, the conditions need to be kept stable for many hours. The induction time before hydrates form can vary from experiment to experiment even if conducted at nominally identical conditions (Natarajan et al., 1994).

The nucleating sites of the gas hydrates in pores directly determine the spatial occurrence and distribution of gas hydrates. Depending on the phase contact in the porous media, the nucleation may occur at the solid-water, and water-gas interfaces in the porous medium (Hawtin et al., 2008). Therefore, the interfacial tensions of these interfaces can determine gas hydrate stability and formation region, which are classified as homogenous nucleation of the spherical and heterogeneous nucleation of cap-shaped (solid-water), lens-shaped (gas-water), and film-shaped according to Fig. 4. Since the gas concentration at the gas–water interface is much higher than that in the bulk solution and due to rock presence as the third phase (foreign substance), gas hydrates mainly tend to be formed in pores, not on substrate surfaces, which indicates the heterogeneous nucleation of gas hydrates as lens-shaped
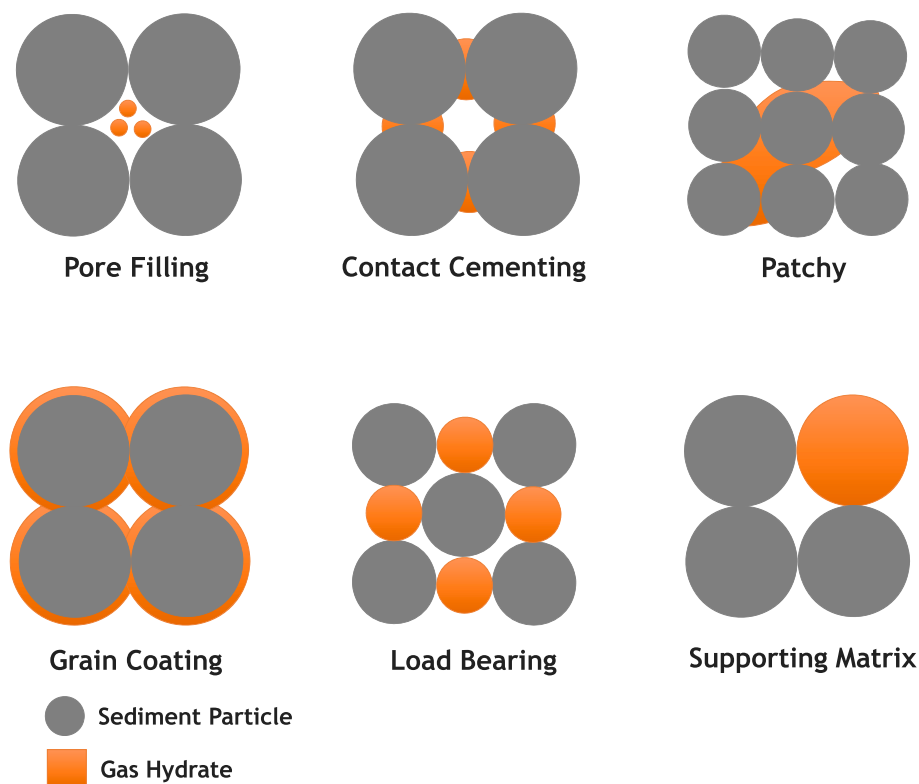
Fig. 3. Morphology of the gas hydrates in porous media. Adapted from (Begum and Satyavani, 2022; Ma et al., 2019):
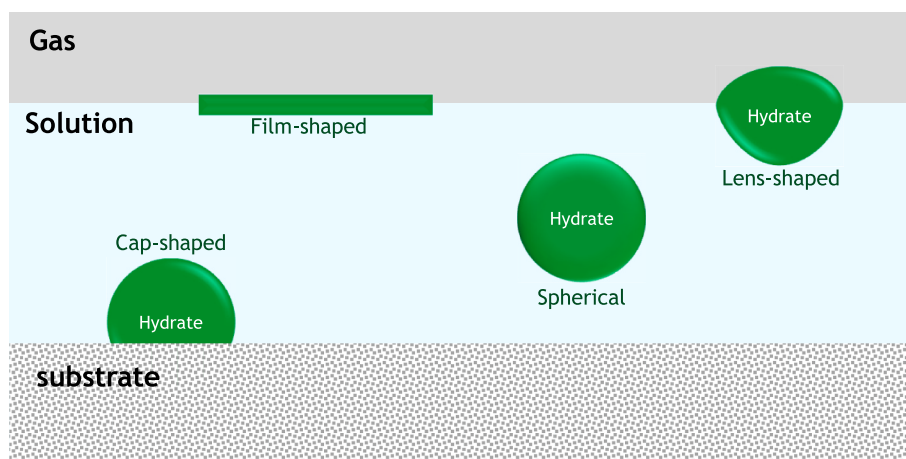

Fig. 4. Potential nucleation sites of the gas hydrates in porous media. Adapted from (Mirzaeifard et al., 2019):

clusters (Zhao et al., 2015b).

The interactions between the main components of the hydrate, i.e., water and gas, are the basis of the three main proposed theories regarding (kinetics of) hydrate formation and dissociation (Lehmkühler et al., 2009).

1. The cluster nucleation theory proposed by Sloan postulated that unstable clusters preferentially agglomerate near the water surface after the dissolution of the gas molecules in the aqueous phase (Sloan and Koh, 2008). When the cluster reaches a critical size, macroscopic nucleation begins.
2. Radhakrishnan and Trout proposed the local structuring theory based on the molecular dynamics (MD) simulation of the dense gas-water interface (Radhakrishnan and Trout, 2002). In this hypothesis, the water and gas molecules are placed stochastically to the point

where a configuration like a hydrate phase is obtained which stabilizes after reaching a certain size and crystals begin to grow.

3. Surface-driven is the third theory introduced by Rodger, which states gas molecules are adsorbed on the water surface and are encapsulated in the middle of relatively constructed water cages (Rodger, 1990).

The physical and chemical characteristics of porous media such as particle size, roughness, wettability, and functional groups have a synergistic effect on the kinetics of CO_2 hydrate (Wang et al., 2022). For instance, surface roughness improves the nucleation sites (Wu et al., 2022). The wettability of surfaces is another property of the porous medium, which has different manifestations depending on the solubility of guest molecules (CO_2). It also impacts the mechanism and kinetics of the gas hydrate nucleation by altering the structure of water molecules

and gas distribution near the connection surface (Bai et al., 2015; Ke et al., 2019). The activity of water confined in the pores could be depressed by the bonding of water molecules with the hydrophilic surfaces of pores, which inhibited hydrate formation (He et al., 2021; Wang et al., 2022). Moreover, a higher degree of wettability results in a shorter induction time for hydrate formation and a faster nucleation rate. Furthermore, the smallest rock particles increase the available specific surface area, provide more area for water distribution, and increase the interfacial contact between multiple points (water-gas-rock). Such a configuration promotes the proliferation of hydrate nucleation sites, giving rise to multiple simultaneous hydrate growth locations (Kvamme et al., 2009).

3.1.2. Impact of pore size on nucleation

The microscopic and macroscopic properties of porous media are strongly affected by the pore size distribution. For example, apart from connectivity of the pores, permeability of a porous medium has a direct relationship with its mean pore size. Therefore, pore size and distribution of pore size along the porous rock are expected to affect hydrate properties. Research has shown that the porous medium with small-diameter pores affects the phase conditions and shifts the hydrate equilibrium curve (Smith et al., 2002). As an example, porous medium with a 4 nm pore diameter displaces the hydrate phase equilibrium to lower temperatures by −12 °C compared to −0.5 °C for the porous medium of 100 nm (Uchida et al., 2002). These effects are mainly due to the additional resistance caused by capillary forces and surface tension between phases, which results in a decrease in the water activity, consequently affecting the hydrate phase boundary. Kang et al. (2008) investigated the hydrate phase equilibrium for CO_2/water systems in various porous media with three pore diameters of 6, 30, and 100 nm and concluded that the pores with 6 nm diameter improved the CO_2 hydrate thermodynamic stability, while the pore with diameter of 30 nm and 100 nm performed inhibition effect in the dissociation equilibria.

A decrease in the grain size potentially increases the rate of hydrate formation. Mekala et al. (2014) conducted CO_2 hydrate formation kinetic experiments in the presence of pure water and seawater (3.3 wt% salinity) using silica beds with three pore sizes. They observed that the CO_2 consumption in hydrate and the induction time of hydrate formation at the end of seawater experiment were both lower than those of the pure-water experiment. A smaller silica size exhibited an enhanced average rate of hydrate formation in the pure-water experiment.

3.1.3. Impact of minerals on hydrate formation

Reservoir rocks, generally sandstone and carbonates, consist of various minerals, such as quartz, kaolinite, bentonite, feldspar, calcite, dolomite, etc., which also play important role in formation and dissociation of hydrates in porous media (Rehman et al., 2021). Compared with sandy sediments, clay sediments are distinguished by an extensive specific surface area through small particle diameters, high capillary pressure, and massive content of bound water, influencing different features of hydrate-formation process (Nair et al., 2016). Mu and Cui investigated the hydrate equilibrium conditions under bulk and clay sediment with various salt content and showed that there is no coupling impact between the clay and salt (Mu and Cui, 2019). They also observed that the temperature changes in the clay and bulk phase were almost identical in the presence of salts. Consequently, due to the stronger interaction forces between the clay and water particles, as well as the water absorption characteristics of the clay that reduce the effective porosity of the sediment through swelling, the coupling impact mostly occurs in the clay-containing systems (Geng et al., 2021). Therefore, the porosity reduction inhibits gas transmission and thus negatively impacts hydrate formation and dissociation (Kumar et al., 2015). Besides, there exist many exchangeable cations among the layered structure of the clays, particularly for bentonite as a lamellar aluminosilicate mineral (Bergaya et al., 2011). Therefore, this specific structure is characterized by its large water absorption capacity, where

water can not only be uptaken into the inner part to bind water but also can create a hydrate structure (Jacobs et al., 2015). The water absorption indirectly increases the free water salinity, resulting in the hydrates formation under more stringent thermodynamic conditions (lower temperatures and higher pressures). A similar result is obtained by Ma et al. (2016) regarding the impact of the amount of the residual water on the hydrate dissociation conditions in the clays, indicating that actual salinity increases, especially when the water content is low owing to binding with clay (Ma et al., 2016).

3.2. Impact of water saturation on hydrate formation

In the bulk phase, when thermodynamic conditions are conducive to CO_2 hydrate formation, the limiting factor lies in the availability of sufficient amounts of water or CO_2. In the CCS projects, CO_2 is continuously supplied to the reservoir, and therefore, the final volume of the hydrate is determined by the water content of the porous formation or water saturation (Benmesbah et al.). Consequently, the water degree affects the spatial availability of sites where hydrates can nucleate, growth and accumulate inside the pore. Moreover, water saturation retards the cold front, and slightly increases the minimum temperature (Chesnokov et al., 2023).

Fig. 5 shows the correlation between hydrate volume and water saturation. The calculations were performed using HydraFLASH software version 3.8 with Soave-Redlich-Kwong (SRK) Equation of State (EoS) for different water saturations at $P = 30$ bar. Hydrate saturation (S_H) was the calculated hydrate volume normalized to the pore volume of the porous medium according to the following equation:

$$m_H = conv \times n_{H_2O}\left(Mw^{H_2O} + \frac{Mw^{CO_2}}{n_H}\right) \quad (2)$$

$$S_H(\%) = \frac{Hydrate\ volume\ (m^3)}{PV\ (m^3)} = \frac{m_H}{PV \times \rho_H} \quad (3)$$

Where m_H is the mass of hydrate, *conv* is the water fraction that has converted to hydrate (%), n_{H_2O}, Mw^{H_2O} and Mw^{CO_2} are the total moles of water, the water and CO_2 molecular weight, respectively. Hydration number (n_H) is the average number of water molecules per guest molecule in the hydrate. In equation (3), the term ρ_H is density of hydrate and *PV* is the pore volume of the porous medium.

There is a linear relationship between hydrate volume (or hydrate saturation or hydrate volume fraction in the porous medium) and water saturation. Hydrate saturation refers to the volume fraction of pore space (containing water and hydrate) occupied by hydrate (You et al., 2019). High water saturation enables a more interconnected network of
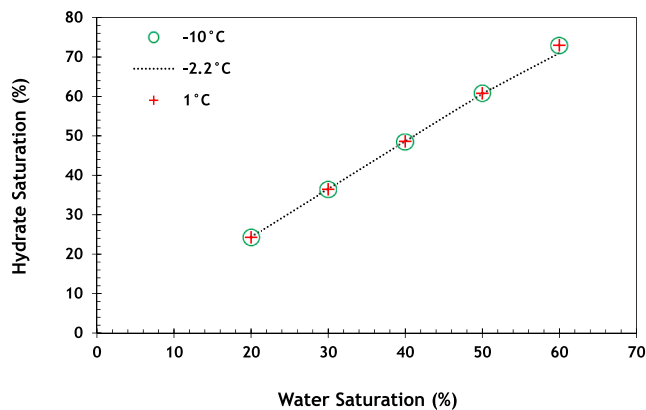

Fig. 5. The relationship between the water saturation and hydrate saturation at different temperatures and *P*=30 bar. At *T*=-10 °C, no ice formation was assumed. The density of the hydrate was calculated as 804.2 ± 0.1 g/L (HydraFLASH version 3.8, SRK EoS).

water molecules, facilitating the construction and accumulation of CO_2 hydrate lattice. However, the impact of S_w on hydrate volume can vary depending on the prevailing thermodynamic conditions of the system, especially at low temperatures when hydrate coexists with the ice. The simulation outcome suggests that when the reservoir conditions fall within the hydrate stability region, the impact of temperature on the volume of hydrate during CO_2 injection is relatively low. This limited influence of temperature could stem from the fact that, when CO_2 concentrations are higher (due to CO_2 inflow), the water is rapidly saturated with CO_2. Consequently, any additional temperature variations do not substantially alter the solubility of CO_2 in water— an essential factor for the formation of hydrates. This insight underscores the complex interplay between temperature, CO_2 concentrations, and water saturation in determining hydrate volume within the porous system.

Furthermore, the temperature profile during cold CO_2 injection is influenced by water saturation, which in turn affects the hydrate stability and phase transitions. The increase in water saturation results in retardation of the cold front, and slight increase of the temperature in the reservoir due to heat content of the water (Mathias et al., 2010). Moreover, considering that the water in the reservoirs usually contains high amounts of salt, hydrate formation has the potential to form concentration gradients and initiate the precipitation of salts or minerals within the pore space of the rock formation, leading to a further reduction in porosity (Zhang and Liu, 2016). The volume of the salt is determined by the volume of the available water in the pores.

3.2.1. Memory effect on formation of hydrates

The water memory effect in the nucleation of gas hydrates refers to the phenomenon that gas hydrates nucleate easier or faster in water that has a history of gas hydrate formation compared to fresh water (water without hydrate history) (Gao et al., 2023; Wei and Maeda, 2023). While research on the water memory effect in bulk systems is relatively abundant (Fandiño and Ruffine, 2014; Uchida et al., 2002; Zhao et al., 2023), its influence on the behavior of CO_2 hydrate in porous media has received less attention due to the complexity of the problem. Based on the molecular hypothesis, the water memory effect can lead to changes in the molecular structure and configuration of the water molecules after dissociation of the CO_2 hydrate. The occurrence of the residual structure is recognized by the difference in water viscosity before hydrate formation and after hydrate dissociation. This altered water structure acts as a kinetic promoter and influences the kinetics of CO_2 hydrate nucleation and growth in the subsequent hydrate formation cycle. For example, the remaining arrangements of the water molecules reinforce the ability of the CO_2 molecules to incorporate into the hydrate lattice or impact the nucleation of the hydrate crystals, when initiated by the pre-existing clusters/structures in water. According to another hypothesis, a significant number of nanobubbles, due to hydrate dissociation in porous media, remain dispersed in the dissociated water for a long time (more than one day). The CO_2–water interfaces of these nanobubbles may act as nucleation sites for heterogeneous nucleation of the hydrate in porous media and subsequently impact the history of distribution/accumulation and growth of the CO_2 hydrate (Hassanpouryouzband et al., 2020; Khurana et al., 2017). Furthermore, the induction time (the duration between the introduction of CO_2 into the system and the first instance of CO_2 hydrate nucleation) is also influenced by the water memory effect (Gauteplass et al., 2020a). This implies that the temporal interval for the onset of the hydrate nucleation can be altered due to the historical interactions of water with its surroundings (Fig. 6).

On the other hand, gas hydrate dissociation is an endothermic process and requires an input of heat energy (depending on the occupancy of the hydrate cage) to break the hydrate structure and release the gas molecules. This energy can be sourced from the surrounding environment, leading to cooling of the system. During subsurface CO_2 storage, the cooling effect resulting from gas hydrate dissociation could establish conditions conducive to the reformation of the new gas hydrates. This is especially relevant if there are residual hydrate structures or memory of
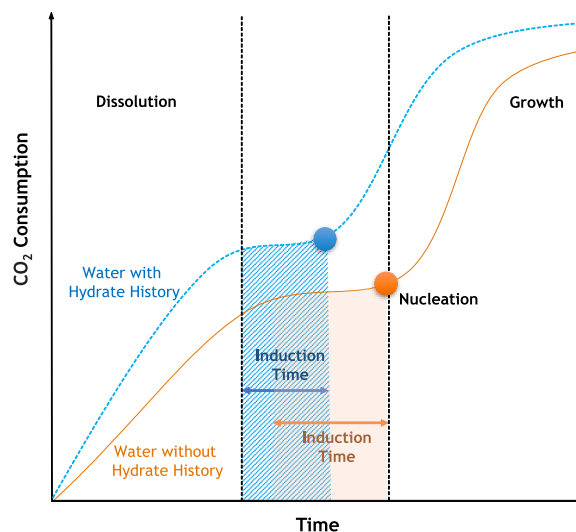

Fig. 6. Representation of memory effect in CO_2 hydrate formation process. All three stages of hydrate formation process (dissolution, induction, and growth) are affected by water memory effect.

previous hydrate formations in the porous medium. This process can lead to a self-sustaining cycle, where dissociation of the existing hydrates triggers formation of new hydrates, especially if there is a continuous supply of gas molecules. This phenomenon can have implications for the stability of the gas hydrates within the reservoir and their potential to reform after dissociation. However, other parameters such as the nature and purity of the guest compound, the mechanism and the temperature of the dissociation, and the specific characteristics of the porous medium all contribute to shaping these changes (Rossi and Gambelli, 2021).

Another hypothesis for water memory effect is the reduced salinity of water with every hydrate formation/dissociation cycle, which affects both CO_2 dissolution and the phase diagram. This is schematically shown in Fig. 7. As only water molecules enter the hydrate structure (Shen et al., 2023), the salinity of the remaining brine increases to the saturation point, such that eventually salt drop out or precipitation occurs in the pores. During dissociation of the hydrate, water molecules exit the lattice; however, due to the limiting mixing and relatively slow rate of salt re-dissolution, for the following hydrate formation cycle the brine salinity is effectively lower. Part of the salt could precipitate in small corners and crevices making the dissolution process even slower. The decrease in salinity increases the CO_2 solubility in brine and promotes hydrate formation in the subsequent cycle.

3.2.2. Self-preservation effect on dissociation

Hydrate self-preservation is interrelated to the ice capping theory (Falenty and Kuhs, 2009), which explains the process of development of a thin liquid water layer on the hydrate surface and subsequently freezing to create an ice cap. This phenomenon could pose another potential challenge concerning the dissociation of CO_2 hydrates, when favorable conditions for hydrate dissociation, such as pressure reduction, arise. Although regasification can be achieved by increasing the temperature above the ice melting point, more extended stability of hydrate within the self-preservation region has been experimentally observed (Li et al., 2021). Due to limited available research, the exact mechanism of self-preservation is obscure, and these knowledge gaps must be comprehended especially for feasible CCS technologies. Under normal conditions, the CO_2 molecules rupture from the hydrate structure, reducing the stability of the hydrate and allowing CO_2 to escape into the gas phase (Kainai et al., 2023; Myshakin et al., 2009; Sum et al., 1997). With self-preservation, the dissociated gas molecules are
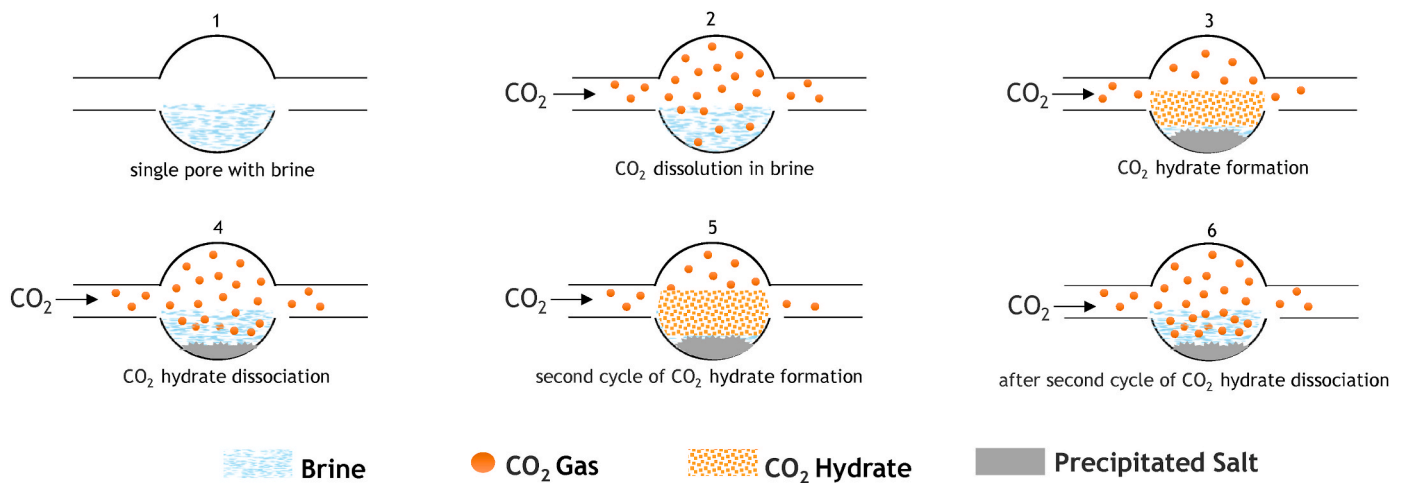
Fig. 7. Impact of water memory on brine salinity and CO_2 hydrate formation/dissociation at the pore scale. The departure of water molecules into the hydrate cage leaves salt behind, which is unlikely to be fully dissolved during dissociation of hydrate. The reduced salinity of the brine enhances hydrate formation in the subsequent cycles.

prevented from leaving the hydrate lattice due to capillary forces that arise from the small pore size of the CO_2 hydrate structure, or a protective layer of the ice around the hydrate particles (Chen et al., 2021; Mestdagh and De Batist, 2015). In the context of subsurface CO_2 storage, this layer can be formed due to heat absorption during hydrate dissociation (endothermic reaction) (Pandey et al., 2021; Singh et al., 2020; Yang et al., 2021) or exposure to cold regions. Indeed, during the dissociation of CO_2 hydrate in the porous media, heat is absorbed by the rock and the in-situ fluids, leading to the formation of a cold or frozen layer in the surrounding layer. This layer acts as a thermal barrier, insulating the remaining CO_2 hydrate from further dissociation (Burla and Pinnelli, 2023; Majid and Koh, 2021). In addition, this cold zone can induce the nucleation of hydrate around the ice layer. This phenomenon is schematically shown in Fig. 8. This condition is more pronounced for higher dissociation rates due to limited time for heat exchange. On the other hand, pore size, geometry, and arrangement are interrelated factors that influence heat transfer in porous media.

3.3. Impact of impurities and mixing on hydrate formation

During CO_2 storage in a depleted gas field, the injected CO_2 will mix with the native gas (usually light hydrocarbons such as CH_4). Moreover, the injected CO_2 stream might contain small traces of other gases. The composition of gas affects both isenthalpic expansion cooling and hydrate properties (Chapoy et al., 2011; Kvamme, 2022). Depending on the specific conditions and the nature of the impurities, the presence of residual impurities can influence CO_2 phase behavior affecting its solubility and miscibility. Consequently, the stability conditions of hydrate

can shift with these variations in pressure and temperature. Moreover, the magnitude of temperature reduction and the position of the cooling front caused by isenthalpic expansion effect is a function of gas composition (Ziabakhsh-Ganji and Kooi, 2014). The macroscopic transport properties of the rock such as relative permeability and capillary pressure function can also be altered by presence of impurities in the gas phase (Anderson et al., 2009).

Fig. 9 compares the thermodynamic conditions of CO_2 hydrate in the presence of impurities with different concentrations inside the reservoir using HydraFLASH software and Cubic Plus Association (CPA) EoS. In the case of H_2S, its higher solubility results in a greater concentration of dissolved H_2S available for hydrate formation. The increased concentration of H_2S can enhance the likelihood of hydrate formation. In addition, H_2S can influence the thermodynamic conditions of the system, impacting the stability conditions for CO_2 hydrate formation, which favors the formation of hydrates at higher temperatures and lower pressures (Mohammadi and Richon, 2015). The presence of N_2 has minimal impact on CO_2 hydrate formation conditions compared to other impurities like CH_4 or H_2S. Since nitrogen does not strongly interact with water molecules or compete for hydrate cage occupancy, its presence has little effect on the stability or formation of CO_2 hydrate. The impact of gaseous impurities on CO_2 hydrate formation conditions tends to be more pronounced at higher pressures. At lower pressures, typically below 40 bar, the solubility of these impurities decreases in the solution, resulting in reduced interaction between the gas and water phases. Consequently, CO_2 hydrate formation is less affected by these gases, and the stability zone is closer to the pure CO_2 phase (the stability zone becomes wider).
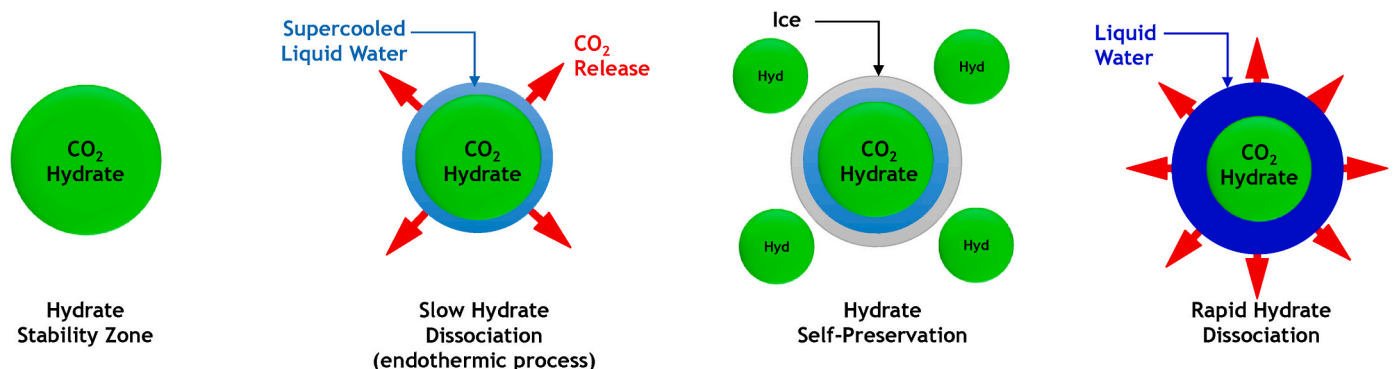

Fig. 8. Self-preservation mechanism impacting the stability of CO_2 hydrate within a porous medium as a result of heat absorption during dissociation of CO_2 hydrate.
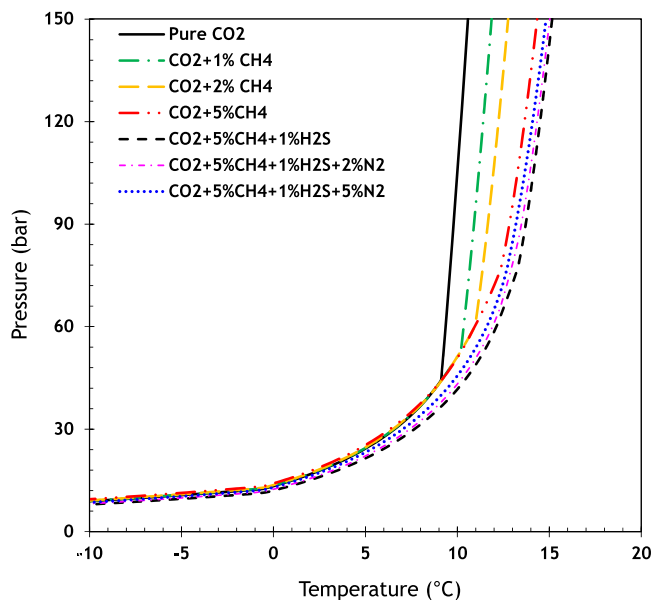
Fig. 9. Thermodynamic conditions of CO2 hydrate in the presence of residual gaseous impurities with 1 wt% NaCl inside the reservoir (HydraFLASH, CPA EoS).

3.4. Impact of capillary heterogeneity

For CO_2 storage applications, it is noteworthy to gain a better understanding of the impact of the geological heterogeneity on the multiphase flow properties of porous media, particularly in the CO_2/ brine distribution during the long-term activity (Saadatpoor et al., 2010). The inherent heterogeneity of the sedimentary rocks gives rise to the issues in the variation of capillary pressure corresponding to local changes in porosity and permeability, for both perspectives of microscopic and macroscopic scenarios. The effect of heterogeneities can be commonly explained by the Leverett J-function and reflected on the P_c – S and k_r – S relationship of a porous medium (Pini et al., 2012). This can be calculated by using the data of the measured capillary pressure. Leverett (1941) gave the scaling relationship of Leverett J-Function for characterizing rock sample capillary heterogeneity:

$$P_c(S_w, k, \varphi) = \sigma \cos \theta \sqrt{\frac{k_{ref}/\varphi_{ref}}{k/\varphi}} J(S_w)$$

where J is the dimensionless J-Function characteristic of a given rock type determined by the measured capillary pressure data, σ and θ are the interfacial tension and contact angle of the fluid systems, φ_{ref} and k_{ref} are the reference porosity and permeability, and φ and k are the porosity and permeability of the rock. Many studies of numerical modeling have revealed that heterogeneity plays a crucial role in CO_2 migration (or CO_2 trapping) and that the permeability dominates the plume migration distance and the sweep area (Han et al., 2010; Nghiem et al., 2009). Residual CO_2 trapping has an inverse function to the permeability, while a higher variance in *lnk* results in an decreased residual trapping.

However, the impact of capillary heterogeneity on hydrate formation is still not well understood. When CO_2 flow encounters a rock, CO_2 displaces the in-situ brine, if the saturation is above the residual or connate water saturation. The non-uniform saturation of water leads to a capillary pressure gradient, that in turn results in back flow of water from the displacement front toward the injectors (Cui et al., 2018). The magnitude of the backflow depends on the shape of the capillary-pressure function, which is determined by the pore size distribution (heterogeneity), and permeability of the rock. The capillary-driven backflow accumulates water close to the injector, which

in contact with the cold CO_2 converts to hydrates. As a result, with more water coming to near wellbore, the saturation of hydrate might increase resulting in more severe injectivity decline. This is similar to the halite precipitation or the dry-out process, which occurs due to the evaporation of water into the gas phase (Talman et al., 2020). Moreover, capillary crossflow can occur between the layers of different permeability, drawing more water from the low permeability layer to the high permeability layer (Roels et al., 2016). For the salt dry-out process, this phenomenon accumulates the brine (and eventually salt) inside the high permeability layer with the highest salt concentration at the interface of the two layers. The capillary pressure gradient is determined by the difference between the layers, the magnitude of the (horizontal and vertical) permeability, while the relative permeability and injection rate determine the magnitude of capillary-driven water backflow and crossflow. These effects are schematically shown in Fig. 10.

It should be noted that because of the key differences between the dynamics of the dry-out and hydrate formation processes, the impact of the capillary-pressure heterogeneity on the two processes could be different and needs further investigation.

3.5. Simultaneous salt dry-out and hydrate formation during CO_2 injection

Under favorable thermodynamic conditions, two processes of salt dry-out and hydrate formation can simultaneously occur in the reservoir during CO_2 injection. However, the interaction between the two competitive phenomena is not well-understood. Research is needed to investigate how the presence of simultaneous salt precipitation and CO_2 hydrate affects mass and heat transport in porous media.

During injection of cold CO_2, the saturations of water, salt, and hydrate vary continuously, at least near the wellbore area. When the temperature of CO_2 is above the hydrate equilibrium temperature, the near wellbore region has temperatures that are outside of the hydrate stability zone (the right region of diagram in Fig. 1). In this case, due to evaporation of water into the gas phase, a dry zone appears. The extent of this dry-out zone depends on reservoir properties, injection rate and salinity of brine. However, when the wellbore temperatures are below the hydrate stability zone, the appearance of the dry-out zone depends on the rates of water evaporation (salt precipitation) and hydrate formation. If evaporation rate is faster, a dry-out zone with high salt concentration might appear. However, the rate of water evaporation is very low at low temperatures, especially when the temperature drops below zero (see Fig. 11). If hydrate formation rate is larger, then hydrates will form first and the available water will be consumed in the hydrate structure. With departure of the water molecules, the brine salinity increases leading to salt precipitation occurring simultaneously in the potential hydrate zone (Liu and Flemings, 2007; Shen et al., 2023). The competition between water evaporation rate and hydrate formation rate needs to be discussed and requires more scientific investigation.

Hydrate formation rate is affected by multiple factors, e.g., temperature and pressure, surface active agents, salinity and ion types, pore size, water saturation, etc. (Zhao et al., 2016). This complexity makes it difficult to quantify the formation rate and to compare it with the loss rate of water. Wells et al. (2021) measured the CO_2 hydrate propagation in a microchannel at a rate over 1000 mm/s, under −2 °C and 400–500 psi. Additionally, the propagation rate increased with the increase in the subcooling temperature and pressure. In porous media, hydrate induction time in salt water is shorter than in pure water but the formation rate is the opposite (Yang et al., 2016). Gauteplass et al. (2018) performed a series of core flooding experiment on the Bentheimer sandstone for three cases of brine salinity, 3.5 wt%, 5 wt% and 7 wt%, under the experimental pressure of 70 bar and temperatures of 4 °C, 6 °C and 7 °C. They observed that after around 0.3 PV of CO_2 injection, the core samples were completely plugged due to hydrate formation. They also noticed that water saturation played an important role on the hydrate formation and pore blockage. In Zhang et al. (2019) experiments were
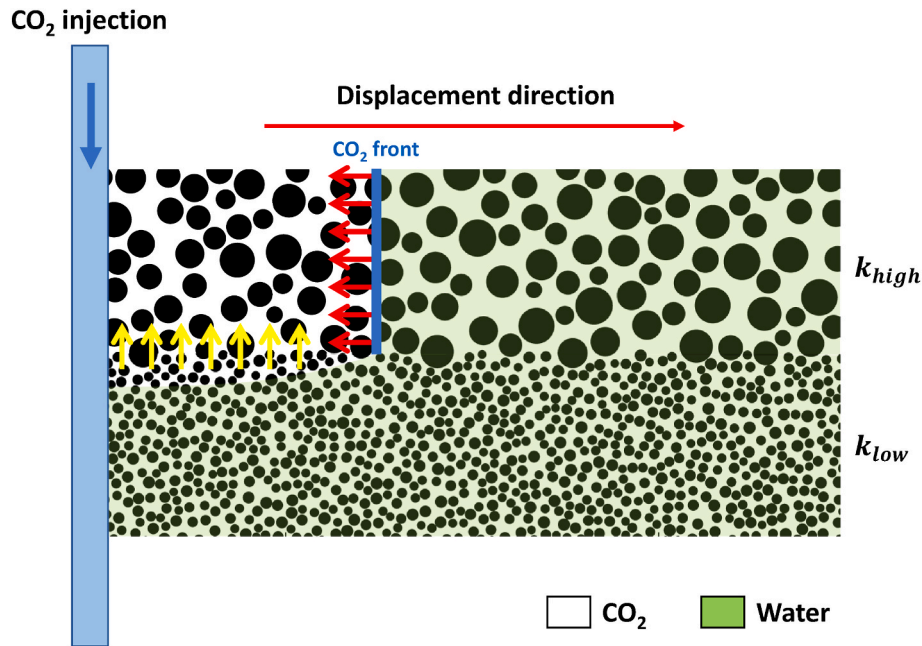
Fig. 10. Schematic of the capillary-driven backflow from high-permeable region to low-permeable region during CO_2 injection. The red arrows present the capillary backflow due to capillary pressure gradient and the yellow arrows present the capillary pressure difference between layers.
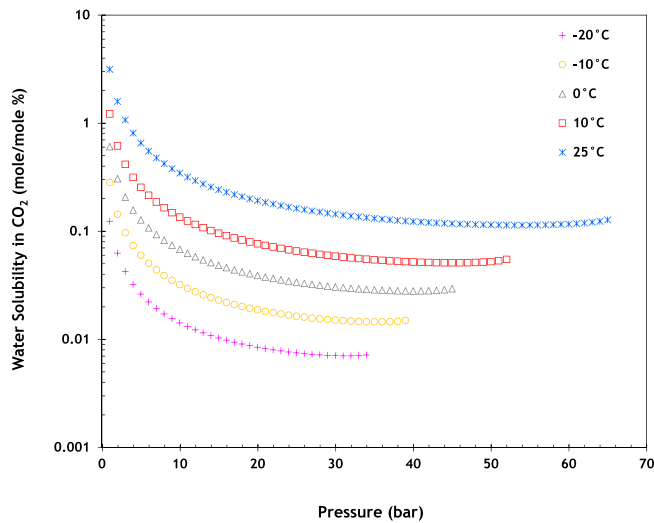

Fig. 11. Water solubility into CO_2 as a function of pressure for various temperatures (data generated using HydraFLASH).

carried out in frozen sand and hydrates were forming from ice (Sice~13%). The formation rates were actually quite low (9.4×10^{-4} mol/h~17 mg/h, and the tests ran for ~140 h to reach a 66% conversion of ice to hydrates).

Furthermore, with evaporation of water, salinity of the reservoir brine starts to increase. The hydrate equilibrium temperature is shifted to lower temperatures. As a result, hydrate formation might be hindered when water evaporation is relatively high.

3.5.1. Impact of hydrate formation on rock permeability

A significant challenge in successful geological storage of CO_2 is the permeability impairment, and ultimately, injectivity loss due to CO_2 hydrate formation in the near-wellbore area. At the early stages of the injection, CO_2 density undergoes a substantial decline due to the dense-to-gas state transition, which subsequently impacts the wellhead

pressure. Consequently, a prompt decrease of the pore space through the ongoing hydrate growth leads to a space blockage and a high-pressure gradient (White, 2011). To mitigate this issue, it is crucial to gain a thorough understanding of the relationship between the permeability and the geometrical features of the porous medium (porosity and permeability), and CO_2 hydrate saturation. Such understanding can provide insights into the mechanisms behind this challenge and aid in developing strategies to prevent or alleviate the adverse effects of CO_2 hydrate formation near the wellbore (Deng et al., 2021; Jianzhong Zhao et al., 2015).

Kneafsey et al. (2011) showed that the permeability of porous sediments appertains to porosity, pore geometry, hydrate morphology, as well as fluid characteristics. Priegnitz et al. (2015) proposed an empirical model, based on which the permeability of the porous medium is mainly influenced by porosity, pore size, and gas hydrate morphology. Hydrate formation in the pore space leads to a decrease in effective permeability, influenced by the hydrate morphology, its distribution and saturation (Sahoo and Best, 2021). In addition, the effective water permeability decreases with the decrease in the pore size, which is further affected by the rock heterogeneity. However, gas-hydrate morphologies that inhibit inner-pore connectivity (switch off pore network pathways) are more than the hydrate morphologies that only confine permeability within pores (reduce flow uniformly through the entire pores network) (see Fig. 3 for illustrations).

Verma and Pruess (1988) proposed a porosity-permeability relationship of the tube-in-series model, which is commonly used in numerical simulations. This model treats capillary as a 1-D tube consisting of wide and narrow segments. The value of the permeability is determined by the local radii of the narrowest part of the tube. Therefore, it can be used for correlating the changes in the permeability and the porosity induced by the clogging in the processes of mineral dissolution and precipitation, shown as

$$\frac{k}{k_0} = \theta^2 \frac{1 - \Gamma + \Gamma/\omega^2}{1 - \Gamma + \Gamma\left(\frac{\theta}{\theta+\omega-1}\right)^2} \tag{4}$$

$$\theta = \frac{\varphi - \varphi_c}{\varphi_0 - \varphi_c} \tag{5}$$

$$\varphi_c = \pi \Gamma \left(\tilde{r}^2 - r^2 \right) \tag{6}$$

where, k_0 and φ_0 are the initial permeability and porosity, θ is the normalized porosity, φ_c is a finite porosity, Γ is the fraction of the total length of a capillary tube has a $\tilde{r}$ while the remainder $1 - \Gamma$ has a smaller radius r, and ω is the ratio of cross sectional areas of the tube segments $(\tilde{r}/r)^2$.

When $\Gamma = 0.8$ and $\varphi_r = 0.9$, is the porosity for the pore radius with r, Equation (2) can be fit by a power law as below (Pruess and Müller, 2009), meaning that the permeability reduces to 0 while 10% of pore space is clogged. The relationship

$$\frac{k}{k_0} = \left(\frac{\frac{\varphi}{\varphi_0} - \varphi_r}{1 - \varphi_r} \right)^2 \tag{7}$$

was proposed as a model in a numerical simulation (Liu et al., 2013). Here, the pore space is considered as cylindrical capillaries with a radii r and was either water-filled or completely dry. The capillary pressure had a relative change with pore volume due to mineral precipitation/dissolution. The permeability change can be described as follows (Le Gallo et al., 1998).

$$\frac{k}{k_0} = \sqrt{\tau} \left[(\delta - 1) \left(1 - \left(1 - \sqrt[m]{S} \right)^m \right) + 1 \right]^2 \tag{8}$$

where τ is the tortuosity factor, and $\tau = 1 - S_p + \delta^2 S_p$, S_p is the effective brine saturation at the time when mineral reaction starts, δ is the multiplied proportionality factor for calculating new pore-size distribution after reactions, and S is the effective water saturation during reactions.

Other correlations have been developed considering different pore shapes than the simple capillary model (e.g., capillary tube model and Kozeny grain model) and the location of hydrates in the pore space (e.g., surface coating and pore-filling), are presented in Table 1.

The permeability calculated by different models are shown in Fig. 12. The pore-filling models appear to allow for full blockage of the pores with formation of hydrates after a certain hydrate saturation.

Additionally, the porosity change with the hydrate formation and accumulation can be described as:

$$\varphi_t = \varphi_i (1 - S_H) \tag{9}$$

where φ_t and φ_i are the total porosity of the porous domain with and without hydrate, respectively (Rempel and Buffett, 1997).

3.5.2. Impact of heterogeneity on permeability reduction

The hydrate nucleation pattern above pore scale level in combination with rock heterogeneity has a major impact on the permeability reduction as illustrated in Fig. 13. The largest permeability reduction is observed for a cross-sectional hydrate pattern (Pan et al., 2021). The

Table 1
Analytical models for water permeability in porous media in the presence of hydrates.

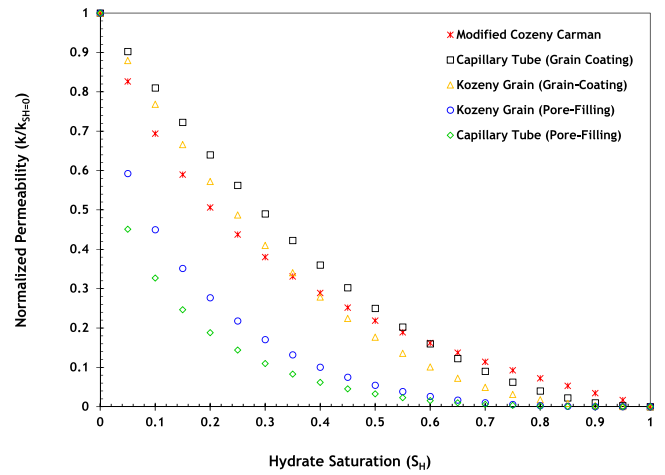| Capillary tube	Grain-coating	$k_{rw} = (1 - S_H)^2$	
	Pore-filling	$k_{rw} = 1 - S_H{}^2 + 2(1 - S_H)^2 / \ln(S_H)$	
Kozeny grain	Grain-coating	$k_{rw} = (1 - S_H)^{n+1}$	if $0 < S_H < 0.8$ then $n^a = 1.5$ it $S_H > 0.8$ then $n^a > 1$
	Pore-filling	$k_{rw} = (1 - S_H)^{n+2}/(1 + S_H{}^{0.5})^2$	$n^a = 0.7\,S_H + 0.3$
	Kozeny-Carman	$k_{rw} = (1 - S_H{}^3)/(1 + 2S_H)^2$	

[a] n: saturation exponent.

Fig. 12. Rock permeability as a function of hydrate saturation – a compilation of analytical models provided in Table 1.

lowest impact is observed in a layered system with layers parallel to flow direction where most of the hydrate is formed in the layers with smaller pores (which have the larger water contents due to higher capillary pressure).

Core flooding experiments imaged by MRI (Ji et al., 2019) suggest that it is possible that eventually the whole pore space of a large-scale rock sample is filled with hydrates, which is the worst case for permeability reduction.

It is important to mention that the larger scale spatial distribution of hydrates is not only a consequence of the rock heterogeneity but also a matter of the injection regime (Shagapov et al., 2015), in a similar way as the dissolution patterns in rock during reactive transport (frontal dissolution, homogeneous dissolution, wormholing etc. (Snippe et al., 2020). For gas hydrate formation, the dominant regimes are based on a conceptual mathematical model (Shagapov et al., 2015) considering volumetric zone, and frontal zone.

However, the initial distribution of the gas is not necessarily uniform. A similar observation was also made by CT scanning (Ji et al., 2019). Note that in the CT scanner, hydrates are identified via their lower density.

3.5.3. Dynamics of well-reservoir interaction

The temperature at the bottomhole depends on the back pressure induced by the porous medium connected to the well (Liu et al., 2016), which is largely determined by the permeability of the rock. The temperature at the sand face decreases with higher permeability. Therefore, for a heterogeneous reservoir with different permeability layers, the high permeability layers will be at higher risk for formation of hydrates due to combined effects of high CO_2 flowrates in these layers and low temperature at the boundary. If the bottomhole temperature is already lower than equilibrium hydrate temperature (see Fig. 15A2), then CO_2 hydrate will form immediately starting from the sand face. Formation of hydrate reduces the rock permeability, resulting in increased pressure in the well (P_1 in Fig. 14), which in turn results in increase of temperature (T_1 in Fig. 14). The speed of pressure increase depends on the rate of hydrate formation and the magnitude of permeability reduction induced by the hydrate. The rock permeability can also be affected by other mechanisms such as salt precipitation, fines migration, dissolution of secondary mineral due to reduced pH, clay swelling, etc. If the temperature rises above the equilibrium hydrate temperature, hydrate will start to dissociate. With the dissociation of hydrate, the reservoir permeability increases, and thus the pressure starts to decline (P_2 in Fig. 14). Hydrate dissociation releases significant volume of CO_2, which can increase the pressure locally. The slope of P_1–P_2 line in Fig. 14 depends on the dissociation rate of the CO_2 hydrate. The rate of
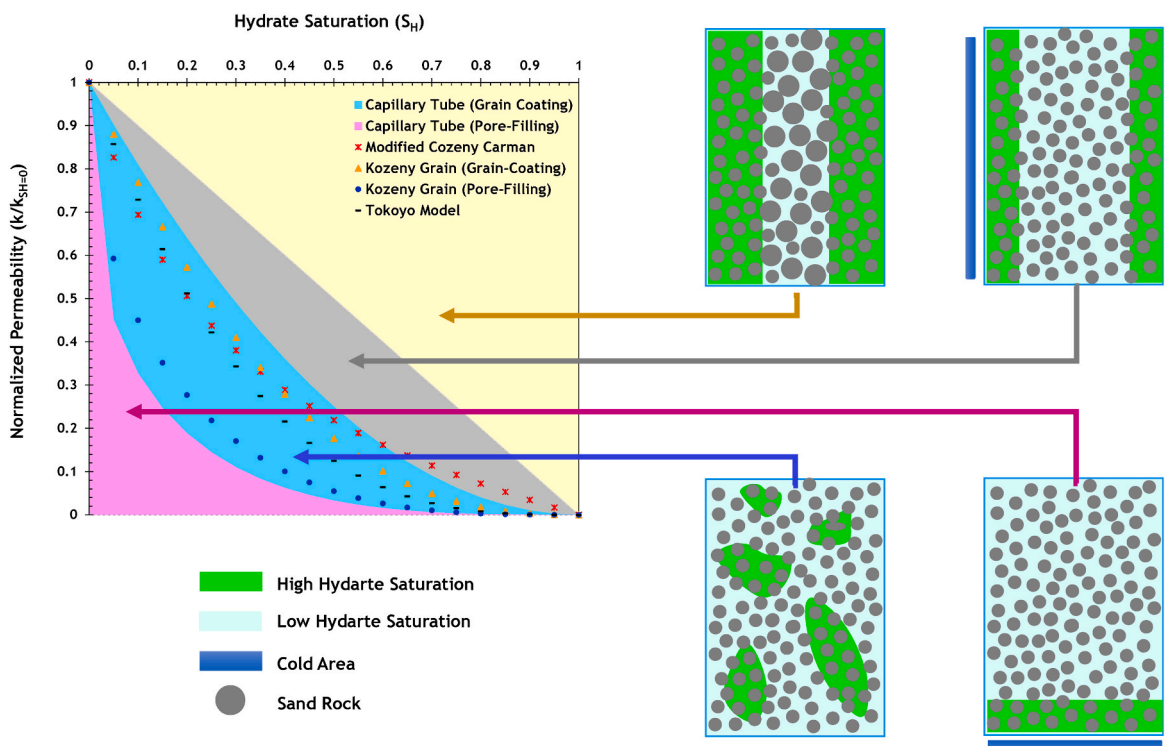
Fig. 13. Impact of the hydrate nucleation pattern and the rock heterogeneity on the permeability reduction. Adopted from (Pan et al., 2021).

dissociation is influenced by injection of hydrate inhibitors (HIs) and thermal stimulation. The extent of heat exchange between the surrounding formations and the hydrate-bearing formation can also affect the rate of dissociation. With the reduction of pressure, the well temperature also comes down. Because of the self-preservation effect, all the encaged CO_2 might not be released, which could result in higher pressure and temperature than those of the previous step. Moreover, with injection of more CO_2 the average reservoir pressure increases. Once again, if the temperature drops below the equilibrium hydrate temperature, hydrate starts to form. Because of the water memory effect, hydrate might form faster in the following cycles with potentially larger volumes or more compact structure.

This dynamic behavior in the boundary between the well and the reservoir continues until the average reservoir pressure increases above the HQP in Fig. 1. The value of the HQP is influenced by many parameters including brine salinity, composition, gas composition, concentration of chemical, etc. At this point, the well temperature stays above the hydrate equilibrium temperature and the situation becomes similar to Fig. 15. For this scenario, formation of hydrate inside the porous medium depends on the magnitude of the pressure drop (which eventually leads to low temperatures due to isenthalpic expansion cooling effect), largely influenced by rock permeability, thickness of the reservoir, injection rate, among other parameters (Mathias et al., 2010). The higher temperature of CO_2 near wellbore can result in faster evaporation of water into the CO_2 stream leading to zone with low water saturation and high salt concentrations.

3.5.4. Multi-scale visualization of hydrate formation in porous media

To detect the formation of hydrates in laboratory experiments, several experimental methods are available. They in general group into Pressure-drop measurements (indirect), and imaging of the hydrates (direct). Pressure-drop measurements utilize the effect of permeability reduction when hydrates form. Even though one of the key questions is the extent of the permeability reduction, the more basic question is whether hydrates are formed in the first place, and how much. Pressure drop is not only impacted by permeability reduction but also by changes

in relative permeability, which also depend on an often-changing water saturation (Ott et al., 2011, 2021).

In addition, in certain types of pore geometries and heterogeneous settings, hydrates may form with hardly an impact on permeability (Ott et al., 2015; Pan et al., 2021). Therefore, pressure drop measurements alone are not considered a reliable method to detect hydrate formation. They provide indications and complementary information is required. To provide a clear and reliable indication of hydrate formation, in-situ monitoring methods are required. Several reliable in-situ imaging methods have been used in the literature including NMR (bulk) (Ji et al., 2019; Vaessen et al., 2000; Zuniga, 2020), MRI (imaging) (Haneda et al., 2002; Ji et al., 2019; Mooijer, 2004), CT – (Meyer et al., 2018), micro-CT (Chaouachi et al., 2015), optical microscopy (2D only) (Lv et al., 2021), electrical resistance (Chen et al., 2020), and Raman spectroscopy (Ikeda et al., 1998, 2018; Nakano et al., 1998; Sum et al., 1997). NMR and MRI are considered very sensitive to the formation of hydrates because the water bound in hydrates is NMR silent (relaxation time is very short), which make hydrates easily and unambiguously detectable (Haneda et al., 2002).

2D-micromodels are usually applied to monitor the hydrate formation and kinetics under controllable observation domain and pore structure (Christiansen and Sloan Jr, 1994; Muraoka et al., 2020; Pandey et al., 2022). The formation of gas hydrates in the 2-D micromodels can be well explained (Wang et al., 2021). Some inside on interactions between wettability, supercooling and hydrate formations and dissociation can be discovered using pedant drop (Daniel-David et al., 2015) and capillary tubes experiments (Touil et al., 2019).

4. CO_2 hydrate prevention/remediation approaches

Gas hydrate controlling techniques (e.g. dehydration, thermal stimulation, and chemical additives, etc) rely on comprehending the mechanisms by which hydrates form and dissociate (Koh et al., 2002; Mooijer, 2004; Peters et al., 2012). In the context of CCS, the utilization of hydrate inhibitors (HIs) represents the most effective and practical chemical approach to control hydrate formation. This involves altering
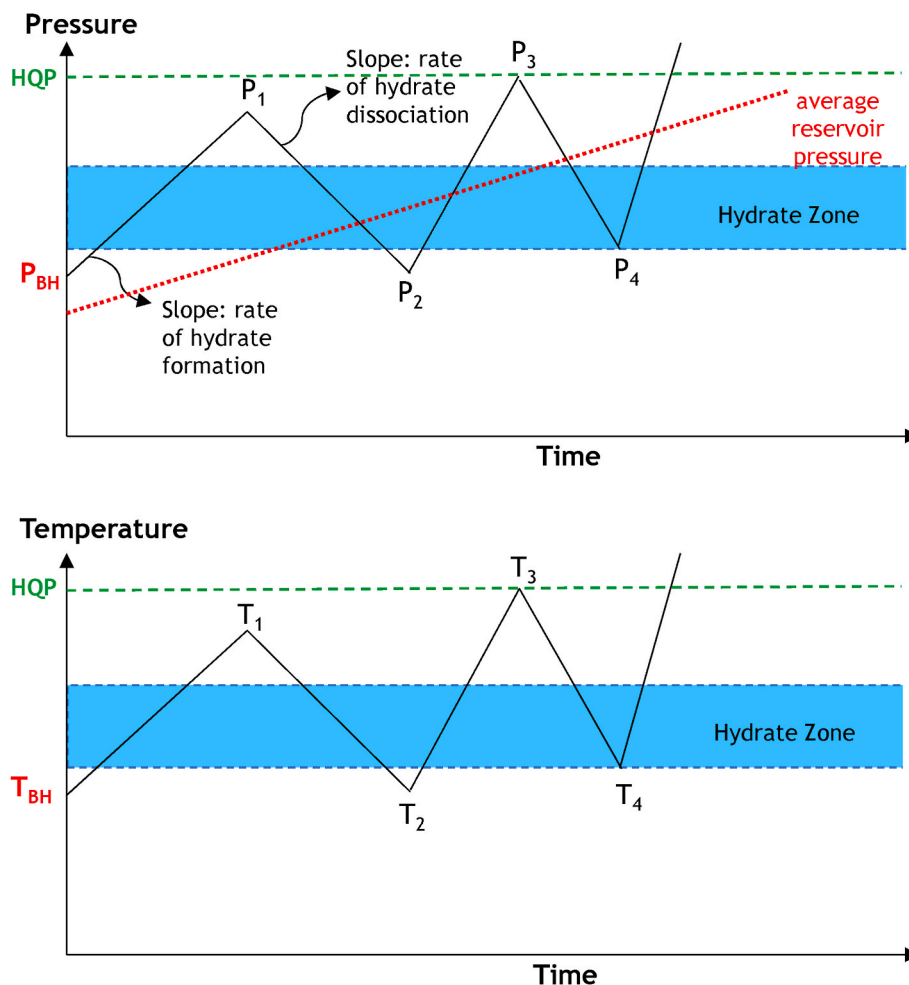
Fig. 14. The continuous change of wellbore temperature and pressure during hydrate formation and dissociation.

hydrate phase boundaries, thereby situating the existing operating conditions outside the Hydrate Stability Zone (HSZ), which is useful in preventing injectivity decline due to the hydrate formation. HIs are segregated into three main groups based on the different inhibition mechanisms, thermodynamic hydrate inhibitors (THIs), kinetic hydrate inhibitors (KHIs), and anti-agglomerates (Ke et al., 2019).

4.1. Impact of thermodynamic hydrate inhibitors (THIs)

Under low water content, THIs is the best chemical to protect the system from hydrate formation by shifting the equilibrium boundary towards lower temperatures or higher pressure (Kelland, 2019; Koh et al., 2012). However, the amount of chemicals required to eliminate the hydrate formation condition may exceed half of the water content. Therefore, their utilization in the CCS project should be considered from two perspectives: (1) functional mechanism and antisolvent effect, (2) economic costs. The THIs can be predominantly classified into three distinct categories: glycols, alcohols, and salts.

4.1.1. Salts (mono and di-valent salts)

Salts or electrolytes are types of THIs that dissociate into cations and anions when dissolved in water and interact with water molecules through strong coulombic attractions which disrupt the hydrogen-bonding network of water and reduce its availability to participate in the hydrate network (Dholabhai et al., 1993; Javanmardi and Moshfe-ghian, 2000; Liu et al., 2021). Smaller ions with higher charge density have a stronger ability to interact and bond with water molecules, showing tendency to disrupt water structure, therefore, hinder hydrate

cage formation (Holzammer et al., 2016; Zhang et al., 2018; Zuo and Stenby, 1997). The hydration of salt ions with water molecules in a saline solution enhances the ion charge, which leads to a decrease in the solubility of nonelectrolyte molecules (CO_2) so-called salting-out effect (Englezos and Bishnoi, 1988; Holzammer et al., 2016; Li et al., 2020). The effectiveness of the salting-out effect depends on the ionic radius of the salt ions, and as the ionic radius increases, the ability of the ions to induce the salting-out effect decreases. This is because larger ions have a weaker influence on water molecules, resulting in weaker solvation and a smaller impact on the solubility of nonelectrolyte molecules. Never-theless, cations and anions can have distinct interactions with water molecules or may form complexes with CO_2 molecules. According to research studies, the inhibition impact of cations on CO_2 hydrate for-mation can be presented in the following order: $Mg^{2+} > Ca^{2+} > Na^+ > K^+$ (Falahieh et al., 2022; Pahlavanzadeh et al., 2023). However, the rela-tive solubility and ionization properties of monovalent (NaCl and KCl) and divalent ($CaCl_2$ and $MgCl_2$) salts in water can indeed have different influences on kinetics, stability, and thermodynamic properties of CO_2 hydrate in distinct ways (Dholabhai et al., 1993; Zha et al., 2012).

Fig. 16 shows the formation conditions of CO_2 hydrate in the pres-ence of single and binary salt solutions using HydraFLASH software. It is seen that increasing salinity of the solution enhances the inhibitory ef-fect on CO_2 hydrate formation, which was observed at both high and low pressures in different saline solutions. However, at high pressures, increasing the solution salinity leads to a more pronounced inhibitory property, resulting in a larger decrease in the hydrate dissociation temperature. Regarding the information provided, at moderate pres-sures and concentrations below 5 wt%, $MgCl_2$ and $CaCl_2$ show a
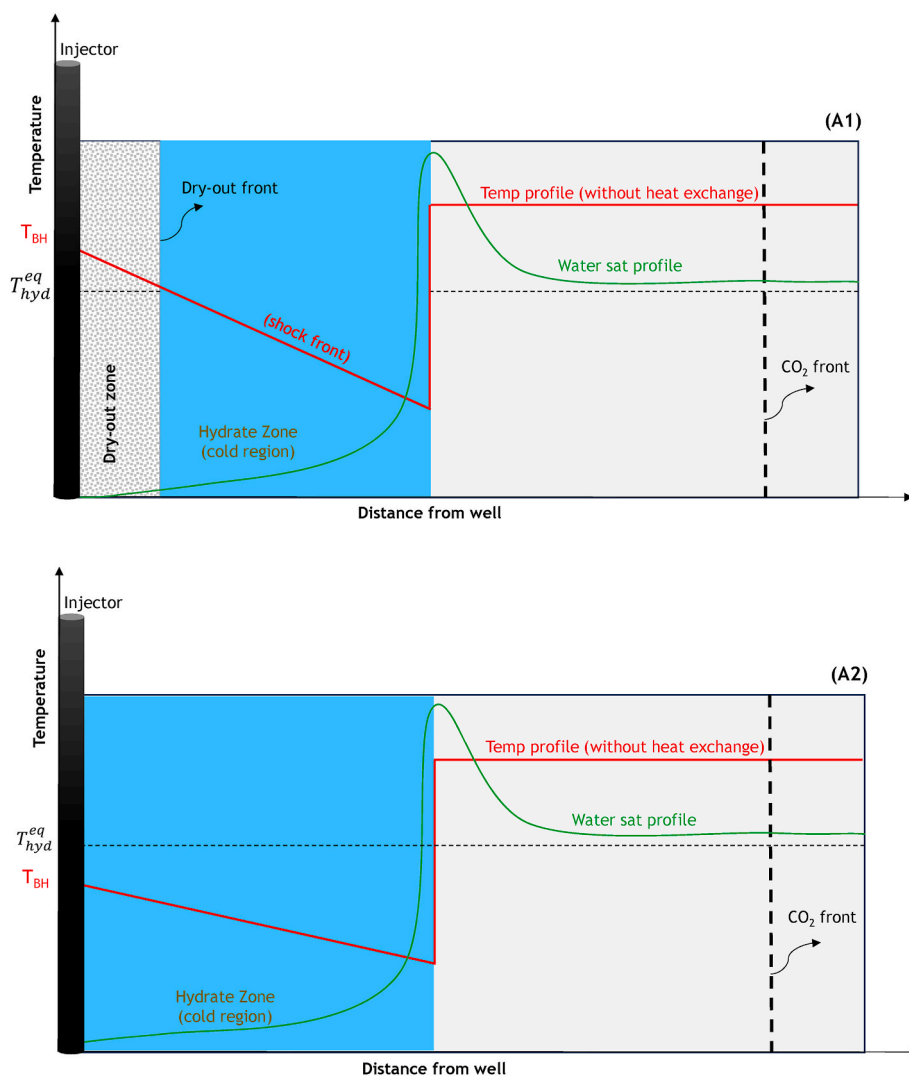
Fig. 15. Impact of wellbore CO_2 temperature on the temperature, water saturation, and hydrate saturation profiles in porous media during injection of cold CO_2.

comparable inhibitory effect on CO_2 hydrate formation. However, at low pressures and concentrations above 10 wt%, $MgCl_2$ demonstrates a greater capacity to decrease the equilibrium temperature of CO_2 hydrate compared to $CaCl_2$. In the binary combination of $NaCl + MgCl_2$, $MgCl_2$ has a stronger inhibitory impact compared to NaCl due to its smaller size and stronger interaction of Mg^{2+} ions with water molecules. On the other hand, in the $NaCl + KCl$ mixture, Na^+ and K^+ ions, being even larger in size, exhibit a relatively lower inhibitory effect due to their weaker interaction with water molecules, however, NaCl exhibits a dominant inhibitory effect.

The presented data is a general trend observed in the laboratory and modeling studies, but the precise impacts can vary under reservoir conditions based on thermodynamic conditions and medium properties. In the scenario where the reservoir experiences a significant drop in temperature, there is a possibility of salt precipitation occurrence. The cooling effect caused by the endothermic dissociation of CO_2 hydrates is another problem that leads to further precipitation of salts, exacerbating the issue. This can lead to the salts losing their effectiveness, especially when operating below their eutectic temperature. In this regard, the maximum concentration of NaCl before precipitation is approximately 23.3 wt% at -21.1 °C, while for a 30 wt% $CaCl_2$ solution, precipitation begins at a lower temperature of -51.5 °C. This parameter can also be impacted by the introduction of other chemicals like MeOH into the reservoir, which can be the subject of future research.

4.1.2. Glycols and alcohols

Research has revealed that reducing the molecular weight (MW) of alcohol or glycol compounds can lead to enhanced performance in suppressing hydrate formation. This effect is attributed to the ability of compounds to form more stable complexes with water or CO_2 molecules. It's noteworthy that, lower-MW inhibitors are generally more efficient as they yield higher molar/molal concentrations than higher-MW inhibitors at the same mass concentration. In this scenario, monoethylene glycol (MEG) exhibits more effective inhibition performance compared to diethylene glycol and triethylene glycol (TEG) due to its lower density and viscosity (Aminnaji et al., 2017; Gauteplass et al., 2020a; Munck et al., 1988; Nielsen and Bucklin, 1983). Moreover, methanol exhibits greater efficacy compared to ethanol. However, one significant drawback of these oxygenated inhibitors, like methanol, is their distribution/evaporation behavior (more volatile/lower boiling temperature), leading to a decrease in their concentration below the desired level compared to non-oxygenated inhibitors like MEG (Brustad et al., 2005). Fig. 17 compares the corresponding weight fraction of different glycols and alcohols as inhibitors for a 10 °C depression temperature of CO_2 hydrate using HydraFLASH. According to the diagram, methanol is preferred due to its strong hydrate inhibition properties, and is often used as selective inhibitors in various applications. However, it should also be worth evaluating other factors such as antisolvent effect, solubility, potential side effects, safety, and economic feasibility when
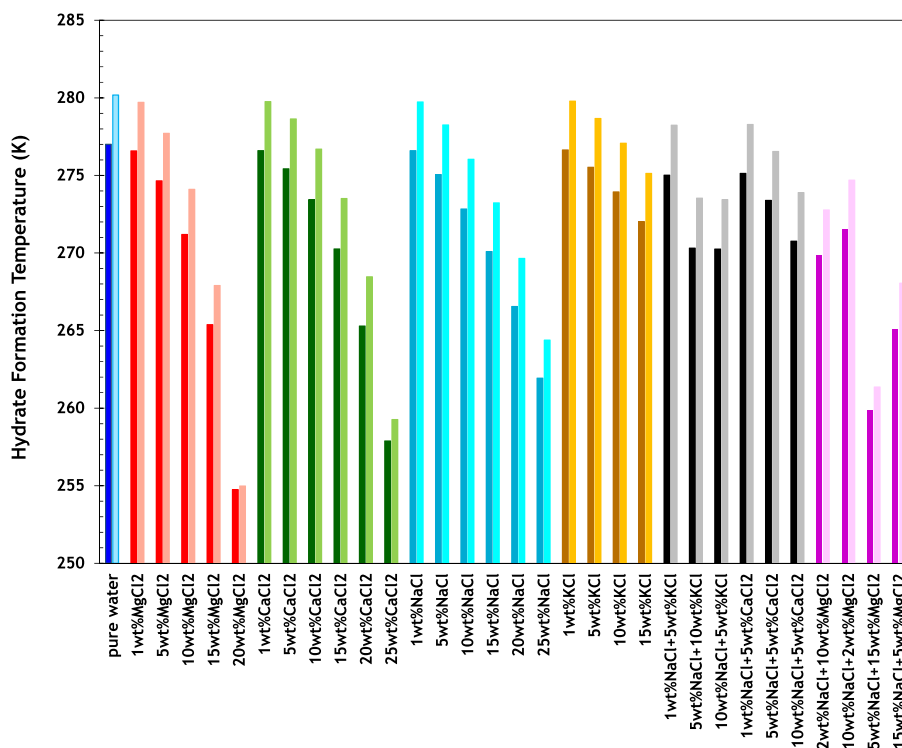
Fig. 16. Impact of different salt types and their concentrations on the CO_2 hydrate equilibrium temperature at elevated pressures. Light column: 30 bar; dark column: 20 bar (HydraFLASH, version 3.8).
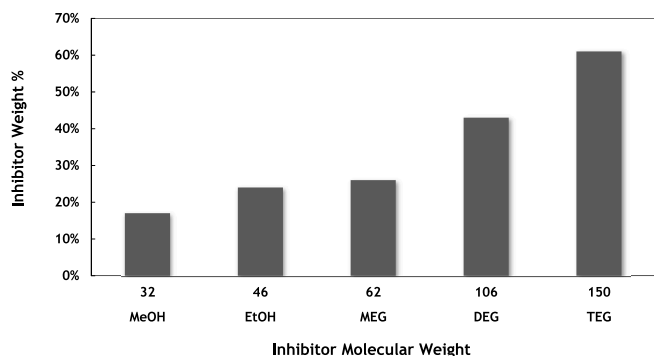

Fig. 17. Inhibitor requirements in the aqueous phase for depression temperature of 10 °C (HydraFLASH version 3.8).

selecting an appropriate inhibitor for CO_2 hydrate inhibition (Cao et al., 2020). The presence of MeOH at low temperature might result in precipitation of salt, that can adversely affect the rock permeability.

In addition, the thermodynamic conditions of CO_2 hydrate in the presence of effective alcohols and glycols have been obtained in a wide range of pressure and concentrations by utilizing HydraFLASH (Fig. 18). Accordingly, the effectiveness of MEG and Methanol can vary depending on their concentration in the system. At low concentrations, the differences in their ability to shift the phase diagram of CO_2 hydrate may be relatively small, and their inhibitory effects may be comparable, while as the concentration increases, the differences in their effectiveness become more pronounced.

Nevertheless, when considering the efficiency of MEG and MeOH as the most efficient and common THI in the context of CCS, the following points should be considered: (1) Due to dissociation of hydrate, the water content of the porous medium increases leading to dilution of MEG or MeOH solutions, which in turn reduces their effectiveness, (2) The temperature drop during CO_2 hydrate dissociation should be
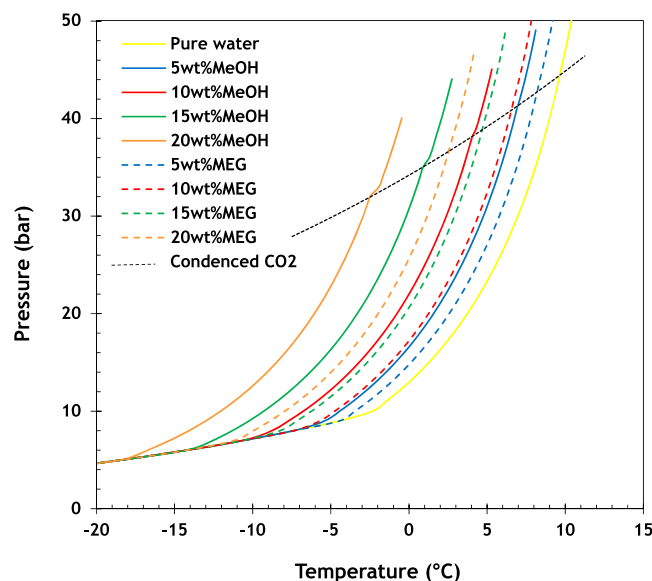
Fig. 18. Impact of Methanol and MEG on hydrate phase of CO2-water system in the absence of additional salt (HydraFLASH v. 3.8).

considered as part of the depression temperature to ensure that operation remains outside HSZ. (3) In terms of THIs selection, MEG is commonly used in gas-dominated systems due to its lower volatility or lower gas solubility compared to MeOH. (4) Due to the viscosity contrast between MEG and water, the mixture might be non-uniform, leading to less contact with the hydrate phase in porous media, which can affect its effectiveness. (5) The rate at which MeOH is injected needs to be aligned with the reservoir's salinity level, as MeOH is not compatible with high-salinity brines, particularly at lower temperatures. With precipitation of the salts, the inhibitory effect of electrolytes becomes less pronounced.

Moreover, the precipitation of salts can also impact the injectivity of CO_2 by reducing the reservoir's porosity/permeability. (6) The compatibility of these chemicals with the reservoir minerals should also be evaluated.

4.2. Impact of kinetic hydrate inhibitors (KHIs)

One of the primary mechanisms of KHIs is the prolongation of the nucleation induction time by adsorption and forming a protective layer or altering the interfacial properties between water and gas phases (Aghajanloo et al., 2022; Bavoh et al., 2016; Li et al., 2019; Sun and Englezos, 2016). When it comes to large-scale subsurface CO_2 storage, the most superiority of KHIs is that they can be applied in relatively small concentrations, typically 0.1 wt% to 1 wt%. This can reduce the cost of materials and investment as well as minimize any potential/side effects of inhibitors on the overall injectivity performance (Kelland, 2019). A major limitation of KHIs in the CCS context is the relatively low degree of subcooling; if subcooling is larger than a specific value (depending on the type of the KHI), the inhibitory property of these chemicals will be greatly diminished, and it may act as a promoter. At low subcooling temperatures pure KHIs are sufficiently effective, while under high subcooling, synergistic HIs may be appropriate (Clarke and Bishnoi, 2005).

The potential KHIs to be applied for CO_2 storage include: (1) Polymeric KHIs such as polyvinylcaprolactam (PVCap), polyvinylpyrrolidone (PVP), which are water-soluble polymers or oligomers that possess both hydrophobic and hydrophilic characteristics (Kelland et al., 2021). The hydrophobic portion of the KHI molecule inhibits hydrate formation by binding to the hydrate cages or occupying specific sites within the water structure (Yagasaki et al., 2015). KHIs reduce the availability of water molecules for hydrate nucleation and inhibit the growth of hydrate crystals. At the same time, the hydrophilic portion of the molecule interacts with water molecules, also reducing the contact surface area between water molecules and CO_2, thus limiting the opportunity for hydrate formation (Liu et al., 2020). However, from a chemical perspective, there are concerns regarding the KHI compounds, potentially adsorbing onto the surface of reservoir rocks. This adsorption could limit their effectiveness and result in increased costs for compensating for the adsorption phenomenon. (2) Biodegradable Inhibitors or environmentally friendly KHIs such as polylactic acid (PLA) and polyhydroxyalkanoates (PHA) that can degrade over time, reducing the long-term impact on the reservoir and surrounding environment. (3) Synergistic combinations of KHIs with THIs such as methanol or MEG to enhance the efficiency and cost-effectiveness of KHIs that have the advantages of both types of inhibitors. The biodegradability and efficacy of the synergistic method can vary depending on the specific combination and the volume fraction of each inhibitor used. Furthermore, unlike THIs, the KHIs performance is time-dependent thus they are mainly applicable to dynamic flow systems, where the hydrate formation and dissociation rates are significant (Yang et al., 2018). The selection of the most suitable KHI for CO_2 storage requires a comprehensive evaluation of factors such as inhibitor performance, compatibility with the CO_2 stream and reservoir properties, cost-effectiveness, and large-scale availability, and operational considerations.

5. Discussion on gaps and future research

Formation of hydrates during injection of cold CO_2 poses potential challenges for low-carbon and cost-effective implementation of CO_2 storage in depleted gas fields. This paper provides a brief review of CO_2 hydrate and its impact on the rock permeability and well injectivity. There have been numerous experimental studies in the literature, which have focused mainly on CH_4 hydrate and more recently on CO_2 hydrate. However, the reported experimental data are not exactly representative of CCS in depleted gas fields. Most of the experiments are designed within the hydrate stability zone, i.e., hydrate formation is forced to form in the porous medium. There are only few reported precedent cases

for hydrate formation at field scale or field-related processes or projects. Most of these examples from the field are scattered and not representative of the conditions of CO_2 injection in depleted gas fields. Nevertheless, these examples demonstrate that in principle CO_2 hydrates or ice can form and, if formed, can significantly impair injectivity. But there is no demonstrated experimental case where CO_2 hydrates form due to J-T cooling during CO_2 injection.

Under non-equilibrium conditions, the hydration number is usually slightly higher than 5.5, indicating that there is 5.5 times more water than CO_2 on a mole fraction basis. This value is influenced by the solubility of CO_2 in liquid water and various thermodynamic conditions. For instance, CO_2 solubility tends to increase significantly with a slight rise in temperature, but it slightly decreases with increasing pressure in the hydrate-water region. As such, the permeability impairment is water-saturation dependent. In the context of continuous CO_2 injection into depleted gas fields, water saturation serves as the limiting factor and prevents hydrate saturation from exceeding a certain threshold. For the water saturations representative of depleted gas fields, the formation of hydrate is expected to partially damage the injectivity. Nevertheless, it is important to note that the formation of CO_2 hydrates is not guaranteed and depends on a variety of factors.

There is a wealth of fundamental studies on many different aspects of hydrate formation where typically one or two parameters are varied at a time. These aspects range from the impact of pressure, temperature, rate, fluid composition, gas composition, impact of mineralogy in particular presence of clays, and the impact of heterogeneity on permeability impairment. Moreover, it is very unlikely that all field conditions can be reproduced in the laboratory to full extent. It is important to realize that pressure, temperature, and compositional gradients in the field are much larger than what can be realized in the laboratory within a single or a combination of experiments. That means that laboratory experiments need to focus on the window in terms of pressure, temperature and other parameters that bear the highest risk for hydrate formation.

Numerical simulations are required to estimate the magnitude of temperature reduction, pressure, and compositional gradients in the field, on which basis the window with the highest risk can be identified (for example by comparison to known bulk behavior for gas hydrates) and reproduced in experiments by active control. Currently, these simulations still have the drawback that they have difficulty with dealing with the continuous phase transitions (gas to liquid, gas to solid, etc). These simulations are still only an estimate of the gradients because these simulations require an input such as permeability reduction as a function of hydrate fraction, which is an outcome of an experimental program (for which these simulations are an input). That means that there is a feedback loop between field scale simulations to estimate the relevant parameter ranges, and the experimental program providing estimates of permeability reduction.

Identification of hydrates in in-situ experiments can pose a significant challenge. Identification on pressure drop alone may not be sufficient, since pressure drop is also influenced by saturation changes and other phenomena such as salt precipitation, thus masking the pressure response. Instead, utilizing imaging equipment such as MRI and CT scanner is recommended.

There is a significant likelihood of false positives and false negatives. This means that the impact of hydrates is not seen in the lab but plays an important role in the reservoir, or hydrate impact is established in the lab but plays no significant role in the reservoir. A field pilot is more likely to address the hydrates risk than laboratory experiments. However, such a pilot needs to have appropriate parameters in terms of temperature and pressure and for calibration of observations may need experimental information that is currently not available in literature.

In combination with the role that heterogeneity plays on the impact of hydrates on permeability reduction, it is not clear which factor in the end dominates with respect to formation and impact on injectivity. That makes the question of the hydrate formation risk very specific to the

actual field situation.

Capillary back flow and cross flow can be driven by the capillary pressure gradient in the process of hydrate formation or salt dry-out and by the capillary pressure difference between heterogeneous reservoir layers, respectively. Water saturation and distribution in the reservoir would have dynamic change that potentially causes the accumulation of hydrate formation near wellbore, which enhances the reduction of CO_2 injectivity. On the other hand, within the processes of hydrate formation or dissociation, reservoir heterogeneity improves the change of local capillary force where alters the thermodynamic conditions and affects hydrate stability. Unstable hydrate gives the uncertain water saturation and distribution and causes change of relative permeability of water. However, few studies have considered the role of heterogeneity in hydrate formation, or elucidated its influence on the wellbore impairment. It is critical to figure out the extent of heterogeneity effect and to tackle the potential problems in the wellbore integrity and injectivity reduction.

When CO_2 temperatures are above the hydrate equilibrium temperature, dry-out may be more pronounced due to increased water evaporation. In some cases, especially when wellbore temperatures are below the hydrate stability threshold, the competition between the water evaporation rate and hydrate formation rate may lead to the precipitation of salts in the reservoir. This can further complicate the dry-out challenges. It is therefore imperative to conduct further research to comprehensively explore the impacts of dry-out and hydrate formation on mass (effective permeability) and heat transport within porous media. Clarifying these interactions will not only advance our fundamental understanding of reservoir behavior during CO_2 injection but also contribute to the development of more effective mitigating strategies for subsurface carbon storage.

The dynamic behavior of hydrate formation and dissociation induces pressure and temperature changes. Hydrate formation near wellbore can cause permeability reduction and therefore pressure and temperature increase in the wellbore. Once the temperature is over the equilibrium hydrate level, hydrate starts to dissociate and release pressure and temperature.

Mitigation strategies (e.g., dehydration, thermal stimulation, and chemical additives, etc.) to eliminate the impact of CO_2 hydrate formation and dissociation are crucial in the context of CCS. Future research efforts should focus on various aspects of this challenge. For instance, the development of novel chemicals that can effectively prevent/inhibit CO_2 hydrate formation to maintain conditions outside of the hydrate stability zone, and to avoid injectivity decline caused by hydrate formation. These inhibitors should meet criteria such as effectiveness, safety, affordability, and biodegradability. Their correct selection is vital for maintaining the integrity of CCS systems during CO_2 injection and storage. Investigating the compatibility of these inhibitors with formation water and reservoir minerals is another key point. Understanding how these chemicals interact with different types of reservoir fluids is also critical for their effective use. Determining the optimal dosage of inhibitors required to effectively prevent CO_2 hydrate formation is essential, especially since recycling these inhibitors from formation water may not be feasible.

Numerical simulation of gas hydrates in porous media has historically faced limitations due to general complexity of the hydrate formation and dissociation processes. This problem requires consistent thermodynamics and chemistry incorporated into thermal-compositional modeling formulation and by construction represents interaction of several physical phenomena performed at different scales. The complexity of the existing models varies from a kinetic description with simplified thermodynamic interactions as in CMG STARS (CMG, 2007) and finishing with the most advanced simulation framework for modeling hydrate dynamics in porous media as in TOUGH-HYDRATE (Yin et al., 2018).

However, it's crucial to acknowledge that the modern hydrate simulation models assume that hydrate formation and dissociation are driven by pressure differences relative to the hydrate equilibrium curve. This assumption is valid within specific regions of the thermodynamic space where three phases (vapor, liquid water, and hydrate) can coexist. In cases with limited brine or gas saturations, hydrate formation can still occur at pressures exceeding those predicted by the equilibrium curve. Furthermore, when modeling hydrate phase equilibria under equilibrium assumptions in TOUGH-HYDRATE, the simulator relies on tabulated equilibrium constants (Moridis, 2003). This approach simplifies the calculation of equilibria but may not capture the dynamic nuances of hydrate behavior under all conditions. Molecular dynamics simulations have also long been proven as a valuable tool, which not only provides insights into molecular phenomena, but is also useful for predicting the macroscopic mechanisms of hydrate formation, dissolution, and stability in porous media (Cheng et al., 2024; Ji et al., 2023).

Rock heterogeneity in combination with non-uniform fluid distribution affects hydrate behavior even at core scale. To deal with hydrate complexity, an effective inversion of core experiments should be performed first and then the modeling results should be regressed to the experimental observations. These observations include pressure measurements at different core locations and dynamic imaging, e.g., CT scans or MRI and allow to inverse the kinetic parameters of hydrate formation at different conditions and parameters. In addition, such model will allow an effective interpolation/extrapolation of experimental results in the parameter space of practical interest for hydrate formation and mitigation.

The developed model needs to be translated then to the reservoir scale. That is not an easy problem since upscaling of the compositional and thermal models are sensitive to the scale of representation. Problems of practical interest often require an effective representation at a coarse scale of almost every component in the governing equations. Several approaches have been proposed for a coarse-scale representation, but most of them are limited to the flow phenomena. In addition, the kinetic description of hydrate formation and dissociation requires to resolve the timescale of the problem when integrating conservation equations. All these time and space sensitivities poses serious challenges to gas hydrate upscaling process.

CRediT authorship contribution statement

Mahnaz Aghajanloo: Writing – original draft, Conceptualization. **Lifei Yan:** Writing – original draft, Conceptualization. **Steffen Berg:** Writing – review & editing. **Denis Voskov:** Writing – review & editing, Supervision, Conceptualization. **Rouhi Farajzadeh:** Writing – review & editing, Writing – original draft, Supervision, Project administration, Methodology, Conceptualization.

Declaration of competing interest

The authors declare that they have no known competing financial interests or personal relationships that could have appeared to influence the work reported in this paper.

Data availability

Data will be made available on request.

Acknowledgement

Nomenclature

AAs	Anti Agglomerates
CCS	Carbon Capture and Sequestration
$Conv_w$	Water Conversion
CPA	Cubic Plus Association
CT	Computed Tomography
DEG	diethylene glycol
EoS	Equation of State
G	Gas
GHSZ	Gas Hydrate Stability Zone
H	Hydrate
HB	Hydrogen Bond
HSZ	Hydrate Stability Zone
HQP	High Quadruple Point
IL	Ionic Liquid
I	Ice
J	dimensionless J-Function
k	permeability
k_0	initial permeability
k_{rw}	relative permeability
k_{ref}	reference permeability
KHIs	Kinetic Hydrate Inhibitors
L	Liquid water
LDHIs	Low Dosage Hydrate Inhibitors
LQP	Low Quadruple Point
m	mass
MD	Molecular Dynamics
MEG	Mono-Ethylene Glycol
ME	Memory Effect
MRI	Magnetic Resonance Imaging
Mw	Molecular Weight
NG	Natural Gas
NMR	Nuclear Magnetic Resonance
n	mole
n_H	hydration number
P	Pressure
P_{BH}	Borehole pressure
Pc	Capillary pressure
PHA	polyhydroxyalkanoates
PLA	polylactic acid
PSD	Pore Size Distribution
PV	Pore Volume
r	radius of capillary tube for the remainder 1-Γ
S	effective water saturation
SRK	Soave Redlich Kwong
S_H	hydrate saturation
S_p	effective brine saturation
S_w	water saturation
T	Temperature
T_{BH}	Borehole temperature
T_{hyd}^{eq}	Equilibrium temperature for hydrate
T_c	critical temperature
TEG	Triethylene Glycole
THIs	Thermodynamic Hydrate Inhibitors
V	vapor
WAG	Water Alternating Gas
wt	mass fraction

Greek Character

ΔH	enthalpy of hydrate formation/dissociation
φ	porosity
$φ_{ref}$	reference porosity
$φ_0$	initial porosity
$φ_c$	finite porosity

φ_r	porosity for the pore radius with r
φ_t	total porosity of the porous domain with hydrate
φ_i	total porosity of the porous domain without hydrate
θ_n	normalized porosity
σ	surface tension
Γ	fraction of the total length of a capillary tube
$\tilde{r}$	radius of capillary tube
ω	ratio of cross sectional areas of the tube segments $(\tilde{r}/r)^2$
τ	tortuosity factor
δ	a multiplied proportionality factor

Subscript & Superscript

BH	Bottom Hole
c	carbon dioxide
eq	equilibrium
H	hydrate
f	final
m	mole
r	relative
t	time
w	water

References

Adeniyi, A.T., Ezeagu, V.I., 2020. *Estimation of Bypassed Oil Volume after Waterflooding an Undersaturated Reservoir* SPE Nigeria Annual International Conference and Exhibition. https://doi.org/10.2118/203656-MS.

Aghajanloo, M., Reza Ehsani, M., Taheri, Z., Jafari Behbahani, T., Mohammadi, A.H., Mohammad Taheri, M., 2022. Kinetics of methane + hydrogen sulfide clathrate hydrate formation in the presence/absence of poly N-vinyl pyrrolidone (PVP) and L-tyrosine: experimental study and modeling of the induction time. Chem. Eng. Sci. 250, 117384 https://doi.org/10.1016/j.ces.2021.117384.

Alavi, S., Woo, T.K., 2007. How much carbon dioxide can be stored in the structure H clathrate hydrates?: a molecular dynamics study. J. Chem. Phys. 126 (4) https://doi.org/10.1063/1.2424936.

Almenningen, S., Graue, A., Ersland, G., 2021. Experimental investigation of critical parameters controlling CH_4–CO_2 exchange in sedimentary CH_4 hydrates. Energy & Fuels 35 (3), 2468–2477. https://doi.org/10.1021/acs.energyfuels.0c03841.

Aminnaji, M., Tohidi, B., Burgass, R., Atilhan, M., 2017. Gas hydrate blockage removal using chemical injection in vertical pipes. J. Nat. Gas Sci. Eng. 40, 17–23. https://doi.org/10.1016/j.jngse.2017.02.003.

Anderson, R., Tohidi, B., Webber, J.B.W., 2009. Gas hydrate growth and dissociation in narrow pore networks: capillary inhibition and hysteresis phenomena. Geological Society, London, Special Publications 319 (1), 145–159. https://doi.org/10.1144/SP319.12.

Bai, D., Chen, G., Zhang, X., Sum, A.K., Wang, W., 2015. How properties of solid surfaces modulate the nucleation of gas hydrate. Sci. Rep. 5 (1), 12747 https://doi.org/10.1038/srep12747.

Ballard, A., Jager, M., Nasrifar, K., Mooijer, M., Peters, C., Sloan, E., 2001. Pseudo-retrograde hydrate phenomena at low pressures. Fluid Phase Equil. 185, 77–87. https://doi.org/10.1016/S0378-3812(01)00458-7.

Bavoh, C.B., Lal, B., Keong, L.K., Jasamai, M., Idress, M.b., 2016. Synergic kinetic inhibition effect of EMIM-Cl + PVP on CO_2 hydrate formation. Procedia Eng. 148, 1232–1238. https://doi.org/10.1016/j.proeng.2016.06.474.

Begum, S., Satyavani, N., 2022. Permeability estimation of gas hydrate-bearing sediments from well log data in the Krishna–Godavari basin. Acta Geophys. 70 (4), 1473–1490. https://doi.org/10.1007/s11600-022-00824-5.

Benmesbah, F., Doria Ruffine, L., Clain, P., Osswald, V., Fandino, O., Fournaison, L., Delahaye, A., 2020. Methane hydrate formation and dissociation in sand media: effect of water saturation, gas flowrate and particle size. Energies 13. https://doi.org/10.3390/en13195200.

Bergaya, F., Jaber, M., Lambert, J.F., 2011. Clays and Clay Minerals. Rubber-Clay Nanocomposites: Science, Technology, and Applications, pp. 1–44.

Brustad, S., Løken, K., Waalmann, J.G., 2005. Hydrate Prevention Using MEG Instead of MeOH: Impact of Experience from Major Norwegian Developments on Technology Selection for Injection and Recovery of MEG. https://doi.org/10.4043/17355-MS.

Bui, M., Adjiman, C.S., Bardow, A., Anthony, E.J., Boston, A., Brown, S., Fennell, P.S., Fuss, S., Galindo, A., Hackett, L.A., Hallett, J.P., Herzog, H.J., Jackson, G., Kemper, J., Krevor, S., Maitland, G.C., Matuszewski, M., Metcalfe, I.S., Petit, C., et al., 2018. Carbon capture and storage (CCS): the way forward. Energy Environ. Sci. 11 https://doi.org/10.1039/c7ee02342a.

Burla, S.K., Pinnelli, P.S.R., 2023. Experimental evidence on the prolonged stability of CO_2 hydrates in the self-preservation region. Case Studies in Chemical and Environmental Engineering 7, 100335. https://doi.org/10.1016/j.cscee.2023.100335.

Cabrera-Ramírez, A., Prosmiti, R., 2022. Modeling of structure H carbon dioxide clathrate hydrates: guest–lattice energies, crystal structure, and pressure

dependencies. J. Phys. Chem. C 126 (35), 14832–14842. https://doi.org/10.1021/acs.jpcc.2c04140.

Cai, W., Huang, X., Lu, H., 2022. Instrumental methods for cage occupancy estimation of gas hydrate. Energies 15 (2), 485. https://www.mdpi.com/1996-1073/15/2/485.

Cao, C., Liu, H., Hou, Z., Mehmood, F., Liao, J., Feng, W., 2020. A review of CO_2 storage in view of safety and cost-effectiveness. Energies 13 (3), 600. https://www.mdpi.com/1996-1073/13/3/600.

Chaouachi, M., Falenty, A., Sell, K., Enzmann, F., Kersten, M., Haberthür, D., Kuhs, W.F., 2015. Microstructural Evolution of Gas Hydrates in Sedimentary Matrices Observed with Synchrotron X-Ray Computed Tomographic Microscopy, vol. 16, pp. 1711–1722. https://doi.org/10.1002/2015GC005811 (6).

Chapoy, A., Burgass, R., Tohidi, B., Austell, J.M., Eickhoff, C., 2011. Effect of common impurities on the phase behavior of carbon-dioxide-rich systems: minimizing the risk of hydrate formation and two-phase flow. SPE J. 16 (4), 921–930. https://doi.org/10.2118/123778-pa.

Chapter 2, 2018. Structural control of nanoparticles. In: Naito, M., Yokoyama, T., Hosokawa, K., Nogi, K. (Eds.), Nanoparticle Technology Handbook, third ed. Elsevier, pp. 49–107. https://doi.org/10.1016/B978-0-444-64110-6.00002-0.

Chen, X., Li, S., Zhang, P., Chen, W., Wu, Q., Zhan, J., Wang, Y., 2021. Promoted disappearance of CO_2 hydrate self-preservation effect by surfactant SDS. Energies 14 (13), 3909. https://www.mdpi.com/1996-1073/14/13/3909.

Chen, Y., Li, K., Han, Y., 2020. Electrical resistance tomography with conditional generative adversarial networks. Meas. Sci. Technol. 31 (5), 055401 https://doi.org/10.1088/1361-6501/ab62c4.

Cheng, L., Li, Y., Cui, J., Wu, Q., Liu, B., Ning, F., Chen, G., 2024. Molecular simulation study on carbon dioxide replacement in methane hydrate near the freezing point. Gas Science and Engineering, 205220. https://doi.org/10.1016/j.jgsce.2024.205220.

Chesnokov, C., Farajzadeh, R., Kahrobaei, S., Snippe, J., Bedrikovetski, P., 2023. Analytical model for joule-thomson cooling under heat exchange during CO_2 storage in geological formations. Int. J. Greenh. Gas Control. https://doi.org/10.2139/ssrn.4441293.

Chong, Z.R., Yang, M., Khoo, B.C., Linga, P., 2016. Size effect of porous media on methane hydrate formation and dissociation in an excess gas environment. Ind. Eng. Chem. Res. 55 (29), 7981–7991. https://doi.org/10.1021/acs.iecr.5b03908.

Christiansen, R.L., Sloan Jr., E.D., 1994. Mechanisms and kinetics of hydrate formation. Ann. N. Y. Acad. Sci. 715 (1), 283–305.

Clarke, M.A., Bishnoi, P.R., 2005. Determination of the intrinsic kinetics of CO_2 gas hydrate formation using in situ particle size analysis. Chem. Eng. Sci. 60 (3), 695–709. https://doi.org/10.1016/j.ces.2004.08.040.

Cui, G., Ren, S., Rui, Z., Ezekiel, J., Zhang, L., Wang, H., 2018. The influence of complicated fluid-rock interactions on the geothermal exploitation in the CO_2 plume geothermal system. Appl. Energy 227, 49–63.

Daniel-David, D., Guerton, F., Dicharry, C., Torré, J.-P., Broseta, D., 2015. Hydrate growth at the interface between water and pure or mixed CO_2/CH_4 gases: influence of pressure, temperature, gas composition and water-soluble surfactants. Chem. Eng. Sci. 132, 118–127.

Davoodi, S., Al-Shargabi, M., Wood, D.A., Rukavishnikov, V.S., Minaev, K.M., 2023. Review of technological progress in carbon dioxide capture, storage, and utilization. Gas Science and Engineering 117, 205070. https://doi.org/10.1016/j.jgsce.2023.205070.

Demirbas, A., 2010. Methane hydrates as potential energy resource: Part 1 – importance, resource and recovery facilities. Energy Convers. Manag. 51 (7), 1547–1561. https://doi.org/10.1016/j.enconman.2010.02.013.

Deng, W., Liang, J., Kuang, Z., Zhang, W., He, Y., Meng, M., Zhong, T., 2021. Permeability prediction for unconsolidated hydrate reservoirs with pore compressibility and porosity inversion in the northern South China Sea. J. Nat. Gas Sci. Eng. 95, 104161.

Dholabhai, P.D., Kalogerakis, N., Bishnoi, P.R., 1993. Equilibrium conditions for carbon dioxide hydrate formation in aqueous electrolyte solutions. J. Chem. Eng. Data 38 (4), 650–654. https://doi.org/10.1021/je00012a045.

Englezos, P., Bishnoi, P.R., 1988. Prediction of gas hydrate formation conditions in aqueous electrolyte solutions. AIChE J. 34, 1718–1721.

Englezos, P., Lee, J.D., 2005. Gas hydrates: a cleaner source of energy and opportunity for innovative technologies. Kor. J. Chem. Eng. 22 (5), 671–681. https://doi.org/10.1007/BF02705781.

Falahieh, M.M., Bonyadi, M., Lashanizadegan, A., 2022. Effect of different salts on the kinetic parameters of the carbon dioxide hydrate formation. J. Nat. Gas Sci. Eng. 100, 104461 https://doi.org/10.1016/j.jngse.2022.104461.

Falenty, A., Kuhs, W.F., 2009. Self-preservation of CO_2 gas hydrates—surface microstructure and ice perfection. J. Phys. Chem. B 113 (49), 15975–15988. https://doi.org/10.1021/jp906859a.

Fandiño, O., Ruffine, L., 2014. Methane hydrate nucleation and growth from the bulk phase: further insights into their mechanisms. Fuel 117, 442–449. https://doi.org/10.1016/j.fuel.2013.10.004.

Farajzadeh, R., Zaal, C., van den Hoek, P., Bruining, J., 2019. Life-cycle assessment of water injection into hydrocarbon reservoirs using exergy concept. J. Clean. Prod. 235, 812–821. https://doi.org/10.1016/j.jclepro.2019.07.034.

Fleyfel, F., Devlin, J.P., 1991. Carbon dioxide clathrate hydrate epitaxial growth: spectroscopic evidence for formation of the simple type-II carbon dioxide hydrate. J. Phys. Chem. 95 (9), 3811–3815. https://doi.org/10.1021/j100162a068.

Gaidukova, O., Misyura, S., Strizhak, P., 2022. Key areas of gas hydrates study: review. Energies 15 (5), 1799. https://www.mdpi.com/1996-1073/15/5/1799.

Gambelli, A.M., Filipponi, M., Rossi, F., 2022. Sequential Formation of CO_2 hydrates in a confined environment: description of phase equilibrium boundary, gas consumption, formation rate and memory effect. Sustainability 14 (14), 8829. https://www.mdpi.com/2071-1050/14/14/8829.

Gao, Q., Zhao, J., Guan, J., Zhang, C., 2023. Influence of the memory effect during CO_2/CH_4 mixed gas hydrate reformation process. Fuel 353, 129249. https://doi.org/10.1016/j.fuel.2023.129249.

Gauteplass, J., Almenningen, S., Barth, T., Ersland, G., 2020a. Hydrate plugging and flow remediation during CO_2 injection in sediments. Energies 13 (17), 4511. https://www.mdpi.com/1996-1073/13/17/4511.

Gauteplass, J., Almenningen, S., Ersland, G., Barth, T., 2018. Hydrate seal formation during laboratory CO_2 injection in a cold aquifer. Int. J. Greenh. Gas Control 78, 21–26. https://doi.org/10.1016/j.ijggc.2018.07.017.

Gauteplass, J., Almenningen, S., Ersland, G., Barth, T., Yang, J., Chapoy, A., 2020b. Multiscale investigation of CO_2 hydrate self-sealing potential for carbon geo-sequestration. Chem. Eng. J. 381, 122646 https://doi.org/10.1016/j.cej.2019.122646.

Geng, L., Cai, J., Lu, C., Qin, X., Qi, R., Meng, F., Xie, Y., Sha, Z., Wang, X., Sun, C., 2021. Phase equilibria of natural gas hydrates in bulk brine and marine sediments from the south China sea. J. Chem. Eng. Data 66 (11), 4064–4074. https://doi.org/10.1021/acs.jced.1c00307.

Han, W.S., Lee, S.Y., Lu, C., McPherson, B.J., 2010. Effects of permeability on CO_2 trapping mechanisms and buoyancy-driven CO_2 migration in saline formations. Water Resour. Res. 46 (7).

Handa, N., Ohsumi, T., 1995. Direct Ocean Disposal of Carbon Dioxide. Terra Scientific Pub. Co.. https://cir.nii.ac.jp/crid/1130000796010100992

Haneda, H., Yamamoto, Y., Komai, T., Aoki, K., Kawamura, T., Ohga, K., 2002. Artificial Roof Construction By the Formation of CO_2 Hydrate in the Development of CH_4 Gas Hydrate Proc. 4th Intnl. Conf. on Gas Hydrates, Yokohama, Japan.

Hassanpouryouzband, A., Joonaki, E., Edlmann, K., Heinemann, N., Yang, J., 2020. Thermodynamic and transport properties of hydrogen containing streams. Sci. Data 7 (1), 222. https://doi.org/10.1038/s41597-020-0568-6.

Hawtin, R.W., Quigley, D., Rodger, P.M., 2008. Gas hydrate nucleation and cage formation at a water/methane interface [10.1039/B807455K]. Phys. Chem. Chem. Phys. 10 (32), 4853–4864. https://doi.org/10.1039/B807455K.

He, Z., Mi, F., Ning, F., 2021. Molecular insights into CO2 hydrate formation in the presence of hydrophilic and hydrophobic solid surfaces. Energy 234, 121260. https://doi.org/10.1016/j.energy.2021.121260.

Holzammer, C., Finckenstein, A., Will, S., Braeuer, A.S., 2016. How sodium chloride salt inhibits the formation of CO_2 gas hydrates. J. Phys. Chem. B 120 (9), 2452–2459. https://doi.org/10.1021/acs.jpcb.5b12487.

Hosseini Zadeh, A., Kim, I., Kim, S., 2021. Characteristics of formation and dissociation of CO_2 hydrates at different CO_2-Water ratios in a bulk condition. J. Petrol. Sci. Eng. 196, 108027 https://doi.org/10.1016/j.petrol.2020.108027.

Hoteit, H., Fahs, M., Soltanian, M.R., 2019. Assessment of CO_2 injectivity during sequestration in depleted gas reservoirs. Geosciences 9 (5), 199. https://doi.org/10.3390/geosciences9050199.

Ikeda, H., Ito, H., Hikita, M., Yamaguchi, N., Uragami, N., Yokoyama, N., Hirota, Y., Kushima, M., Ajioka, Y., Inoue, H., 2018. Raman spectroscopy for the diagnosis of unlabeled and unstained histopathological tissue specimens. World J. Gastrointest. Oncol. 10 (11), 439–448. https://doi.org/10.4251/wjgo.v10.i11.439.

Ikeda, T., Mae, S., Uchida, T., 1998. Effect of guest–host interaction on Raman spectrum of a CO_2 clathrate hydrate single crystal. J. Chem. Phys. 108 (4), 1352–1359. https://doi.org/10.1063/1.475508.

Jacobs, P.J., Hemdane, S., Dornez, E., Delcour, J.A., Courtin, C.M., 2015. Study of hydration properties of wheat bran as a function of particle size. Food Chem. 179, 296–304.

Jadhawar, P., Mohammadi, A.H., Yang, J., Tohidi, B., 2006. Subsurface Carbon Dioxide Storage through Clathrate Hydrate Formation. Advances in the Geological Storage of Carbon Dioxide. Dordrecht.

Jasamai, M., Idress, M., Saaid, I.M., Sabil, K.M., 2016. Effect of Water Saturation on Relative Permeability and Porosity in Hydrate Bearing Sand. International Petroleum Technology Conference.

Javanmardi, J., Moshfeghian, M., 2000. A new approach for prediction of gas hydrate formation conditions in aqueous electrolyte solutions. Fluid Phase Equil. 168 (2), 135–148. https://doi.org/10.1016/S0378-3812(99)00322-2.

Jensen, T.B., Harpole, K.J., Østhus, A., 2000. EOR Screening for Ekofisk. SPE European Petroleum Conference.

Ji, Y., Hou, J., Cui, G., Lu, N., Zhao, E., Liu, Y., Du, Q., 2019. Experimental study on methane hydrate formation in a partially saturated sandstone using low-field NMR technique. Fuel 251, 82–90.

Ji, Z., He, C., Sun, Y., Yue, X., Fang, H., Lu, X., Liu, S., Lyu, W., 2023. Molecular dynamics simulation of CO_2 storage in reservoir pores with a dead-end. Energies 16 (21), 7341. https://www.mdpi.com/1996-1073/16/21/7341.

Kainai, D., Zhang, J., Bai, D., 2023. The melting kinetics of gas hydrate with different cage occupancy and empty cage distribution. J. Mol. Liq. 370, 121006 https://doi.org/10.1016/j.molliq.2022.121006.

Kang, S.P., Lee, J.W., Ryu, H.J., 2008. Phase behavior of methane and carbon dioxide hydrates in meso- and macro-sized porous media. Fluid Phase Equil. 274 (1–2), 68–72. https://doi.org/10.1016/j.fluid.2008.09.003.

Ke, W., Svartaas, T.M., Chen, D., 2019. A review of gas hydrate nucleation theories and growth models. J. Nat. Gas Sci. Eng. 61, 169–196. https://doi.org/10.1016/j.jngse.2018.10.021.

Kelland, M.A., 2019. Challenges with gas hydrate formation. IOP Conf. Ser. Mater. Sci. Eng. 700 (1), 012057 https://doi.org/10.1088/1757-899X/700/1/012057.

Kelland, M.A., Zhang, Q., Dirdal, E.G., Mady, M.F., 2021. Reliability and performance of vinyl lactam-based kinetic hydrate inhibitor polymers after treatment under a range of conditions. Energy & Fuels 35 (2), 1273–1280. https://doi.org/10.1021/acs.energyfuels.0c03519.

Khurana, M., Yin, Z., Linga, P., 2017. A review of clathrate hydrate nucleation. ACS Sustain. Chem. Eng. 5 (12), 11176–11203. https://doi.org/10.1021/acssuschemeng.7b03238.

Kneafsey, T.J., Seol, Y., Gupta, A., Tomutsa, L., 2011. Permeability of laboratory-formed methane-hydrate-bearing sand: measurements and observations using X-ray computed tomography. SPE J. 16 (1), 78–94.

Koh, C.A., Sloan, E.D., Sum, A.K., Wu, D.T., 2011. Fundamentals and applications of gas hydrates. Annu. Rev. Chem. Biomol. Eng. 2, 237–257.

Koh, C.A., Sum, A.K., Sloan, E.D., 2012. State of the art: natural gas hydrates as a natural resource. J. Nat. Gas Sci. Eng. 8, 132–138. https://doi.org/10.1016/j.jngse.2012.01.005.

Koh, C.A., Westacott, R.E., Zhang, W., Hirachand, K., Creek, J.L., Soper, A.K., 2002. Mechanisms of gas hydrate formation and inhibition. Fluid Phase Equil. 194–197, 143–151. https://doi.org/10.1016/S0378-3812(01)00660-4.

Kumar, A., Sakpal, T., Kumar, R., Roy, S., 2015. Methane hydrate formation in a test sediment of sand and clay at various levels of water saturation. Can. J. Chem. 93 (8), 874–881. https://inis.iaea.org/search/search.aspx?orig_q=RN:50024653.

Kumar, R., Englezos, P., Moudrakovski, I., Ripmeester, J.A., 2009. Structure and composition of CO_2/H_2 and CO_2/H_2/C_3H_8 hydrate in relation to simultaneous CO_2 capture and H_2 production. AIChE J. 55 (6), 1584–1594. https://doi.org/10.1002/aic.11844.

Kvamme, B., 2022. Mechanisms for CH_4/CO_2 swapping in natural sediments. Fluids 7 (8), 260. https://www.mdpi.com/2311-5521/7/8/260.

Kvamme, B., Aromada, S.A., Saeidi, N., Hustache-Marmou, T., Gjerstad, P., 2020. Hydrate nucleation, growth, and induction. ACS Omega 5 (6), 2603–2619. https://doi.org/10.1021/acsomega.9b02865.

Kvamme, B., Graue, A., Buanes, T., Kuznetsova, T., Ersland, G., 2009. Effects of solid surfaces on hydrate kinetics and stability. Geological Society, London, Special Publications 319 (1), 131–144. https://doi.org/10.1144/SP319.11.

Le Gallo, Y., Bildstein, O., Brosse, E., 1998. Coupled reaction-flow modeling of diagenetic changes in reservoir permeability, porosity and mineral compositions. J. Hydrol. 209 (1–4), 366–388.

Lederhos, J.P., Long, J.P., Sum, A., Christiansen, R.L., Sloan, E.D., 1996. Effective kinetic inhibitors for natural gas hydrates. Chem. Eng. Sci. 51 (8), 1221–1229. https://doi.org/10.1016/0009-2509(95)00370-3.

Lee, J., Mok, J., Choi, W., Seo, Y., 2023. Influence of structural transformation on guest exchange behavior in the sII hydrate – (CO_2 + N_2) replacement for energy recovery and CO_2 sequestration. Chem. Eng. J. 472, 144680 https://doi.org/10.1016/j.cej.2023.144680.

Lehmkühler, F., Paulus, M., Sternemann, C., Lietz, D., Venturini, F., Gutt, C., Tolan, M., 2009. The carbon Dioxide−Water interface at conditions of gas hydrate formation. J. Am. Chem. Soc. 131 (2), 585–589. https://doi.org/10.1021/ja806211r.

Leverett, M., 1941. Capillary behavior in porous solids. Transactions of the AIME 142 (1), 152–169.

Levin, K., Boehm, S., Carter, R., 6 Big findings from the IPCC, 2022. Report on Climate Impacts, Adaptation and Vulnerability.

Li, M., Fan, S., Wang, Y., Lang, X., Li, G., Wang, S., Yu, C., 2022. Effect of surface curvature and wettability on nucleation of methane hydrate. AIChE J. 68 (10), e17823 https://doi.org/10.1002/aic.17823.

Li, X.-Y., Zhong, D.-L., Englezos, P., Lu, Y.-Y., Yan, J., Qing, S.-L., 2021. Insights into the self-preservation effect of methane hydrate at atmospheric pressure using high pressure DSC. J. Nat. Gas Sci. Eng. 86, 103738 https://doi.org/10.1016/j.jngse.2020.103738.

Li, Y., Maria Gambelli, A., Chen, J., Yin, Z., Rossi, F., Tronconi, E., Mei, S., 2023. Experimental study on the competition between carbon dioxide hydrate and ice below the freezing point. Chem. Eng. Sci. 268, 118426 https://doi.org/10.1016/j.ces.2022.118426.

Li, Y., Qiao, Z., Sun, S., Zhang, T., 2020. Thermodynamic modeling of CO_2 solubility in saline water using NVT flash with the cubic-Plus-association equation of state. Fluid Phase Equil. 520, 112657 https://doi.org/10.1016/j.fluid.2020.112657.

Li, Z., Liao, K., Qin, H.-B., Chen, J., Ren, L., Li, F., Zhang, X., Liu, B., Chen, G., 2019. The gas-adsorption mechanism of kinetic hydrate inhibitors. AIChE J. 65 (9), e16681 https://doi.org/10.1002/aic.16681.

Liu, F.P., Li, A.R., Qing, S.L., Luo, Z.D., Ma, Y.L., 2022. Formation kinetics, mechanism of CO_2 hydrate and its applications. Renew. Sustain. Energy Rev. 159, 112221 https://doi.org/10.1016/j.rser.2022.112221.

Liu, H.-H., Zhang, G., Yi, Z., Wang, Y., 2013. A permeability-change relationship in the dryout zone for CO_2 injection into saline aquifers. Int. J. Greenh. Gas Control 15, 42–47.

Liu, J., Wang, H., Guo, J., Chen, G., Zhong, J., Yan, Y., Zhang, J., 2020. Molecular insights into the kinetic hydrate inhibition performance of Poly(N-vinyl lactam) polymers. J. Nat. Gas Sci. Eng. 83, 103504 https://doi.org/10.1016/j.jngse.2020.103504.

Liu, X., Falcone, G., Teodoriu, C., 2016. Liquid loading in gas wells: experimental investigation of back pressure effects on the near-wellbore reservoir. J. Nat. Gas Sci. Eng. 36, 434–441. https://doi.org/10.1016/j.jngse.2016.10.064.

Liu, X., Flemings, P.B., 2007. Dynamic multiphase flow model of hydrate formation in marine sediments. J. Geophys. Res. Solid Earth 112 (B3). https://doi.org/10.1029/2005JB004227.

Liu, Y., Zhang, L., Yang, L., Dong, H., Zhao, J., Song, Y., 2021. Behaviors of CO_2 hydrate formation in the presence of acid-dissolvable organic matters. Environ. Sci. Technol. 55 (9), 6206–6213. https://doi.org/10.1021/acs.est.0c06407.

Loeve, D., Hofstee, C., Maas, J.G., 2014. Thermal effects in a depleted gas field by cold CO_2 injection in the presence of methane. Energy Proc. 63, 3632–3647. https://doi.org/10.1016/j.egypro.2014.11.393.

Lv, J., Xue, K., Zhang, Z., Cheng, Z., Liu, Y., Mu, H., 2021. Pore-scale investigation of hydrate morphology evolution and seepage characteristics in hydrate bearing microfluidic chip. J. Nat. Gas Sci. Eng. 88, 103881 https://doi.org/10.1016/j.jngse.2021.103881.

Ma, S., Zheng, J.-n., Tang, D., Li, Y., Li, Q., Lv, X., 2019. Application of X-ray computed tomography technology in gas hydrate. Energy Technol. 7 (6), 1800699 https://doi.org/10.1002/ente.201800699.

Ma, Z.W., Zhang, P., Bao, H.S., Deng, S., 2016. Review of fundamental properties of CO_2 hydrates and CO2 capture and separation using hydration method. Renew. Sustain. Energy Rev. 53, 1273–1302. https://doi.org/10.1016/j.rser.2015.09.076.

Majid, A.A.A., Koh, C.A., 2021. Self-preservation phenomenon in gas hydrates and its application for energy storage. In: Bernstein, E.R. (Ed.), Intra- and Intermolecular Interactions between Non-covalently Bonded Species. Elsevier, pp. 267–285. https://doi.org/10.1016/B978-0-12-817586-6.00008-6.

Maloney, D., Briceno, M., 2009. Experimental investigation of cooling effects resulting from injecting high pressure liquid or supercritical CO_2 into a low pressure gas reservoir. Petrophysics 50, 335–344.

Martinez, C., Sandoval, J.F., Ortiz, N., Ovalle, S., Beltran, J.G., 2022. Mechanisms, growth rates, and morphologies of gas hydrates of carbon dioxide, methane, and their mixtures. Methane 1 (1), 2–23. https://www.mdpi.com/2674-0389/1/1/2.

Mathias, S.A., Gluyas, J.G., Oldenburg, C.M., Tsang, C.F., 2010. Analytical solution for Joule–Thomson cooling during CO_2 geo-sequestration in depleted oil and gas reservoirs. Int. J. Greenh. Gas Control 4 (5), 806–810. https://doi.org/10.1016/j.ijggc.2010.05.008.

Mekala, P., Busch, M., Mech, D., Patel, R.S., Sangwai, J.S., 2014. Effect of silica sand size on the formation kinetics of CO_2 hydrate in porous media in the presence of pure water and seawater relevant for CO_2 sequestration. J. Petrol. Sci. Eng. 122, 1–9. https://doi.org/10.1016/j.petrol.2014.08.017.

Mestdagh, T., De Batist, M., 2015. Evaluation and Modelling of the Response of Gas Hydrate Reservoirs to Changing Environmental Conditions across a High-Latitude Continental Margin.

Meyer, D.W., Flemings, P.B., DiCarlo, D., 2018. Effect of gas flow rate on hydrate formation within the hydrate stability zone. J. Geophys. Res. Solid Earth 123 (8). https://doi.org/10.1029/2018JB015878.

Mirzaeifard, S., Servio, P., Rey, A.D., 2019. Characterization of nucleation of methane hydrate crystals: interfacial theory and molecular simulation. J. Colloid Interface Sci. 557, 556–567. https://doi.org/10.1016/j.jcis.2019.09.056.

Mohammadi, A.H., Richon, D., 2015. Hydrate phase equilibria of gaseous mixtures of methane + carbon dioxide + hydrogen sulfide. Chem. Eng. Commun. 202 (5), 629–633. https://doi.org/10.1080/00986445.2013.858322.

Mooijer, M., 2004. Phase Behaviour and Structural Aspects of Ternary Clathrate Hydrate Systems.

Moridis, G.J., 2003. Numerical studies of gas production from methane hydrates. SPE J. 8 (4), 359–370. https://doi.org/10.2118/87330-pa.

Mu, L., Cui, Q., 2019. Experimental study on the dissociation equilibrium of (CH_4+ CO_2+ N_2) hydrates in the mixed sediments. J. Chem. Eng. Data 64 (12), 5806–5813.

Munck, J., Skjold-Jørgensen, S., Rasmussen, P., 1988. Computations of the formation of gas hydrates. Chem. Eng. Sci. 43 (10), 2661–2672. https://doi.org/10.1016/0009-2509(88)80010-1.

Muraoka, M., Yamamoto, Y., Tenma, N., 2020. Simultaneous measurement of water permeability and methane hydrate pore habit using a two-dimensional glass micromodel. J. Nat. Gas Sci. Eng. 77, 103279.

Myshakin, E.M., Jiang, H., Warzinski, R.P., Jordan, K.D., 2009. Molecular dynamics simulations of methane hydrate decomposition. J. Phys. Chem. 113 (10), 1913–1921.

Nagashima, H., Miyagi, T., Yasuda, K., Ohmura, R., 2020. Clathrate hydrates at temperatures below the freezing point of water: a review. Fluid Phase Equil. 517, 112610 https://doi.org/10.1016/j.fluid.2020.112610.

Nair, V.C., Ramesh, S., Ramadass, G.A., Sangwai, J.S., 2016. Influence of thermal stimulation on the methane hydrate dissociation in porous media under confined reservoir. J. Petrol. Sci. Eng. 147, 547–559. https://doi.org/10.1016/j.petrol.2016.09.017.

Nakano, S., Moritoki, M., Ohgaki, K., 1998. High-pressure phase equilibrium and Raman microprobe spectroscopic studies on the CO_2 hydrate system. J. Chem. Eng. Data 43 (5), 807–810.

Natarajan, V., Bishnoi, P.R., Kalogerakis, N., 1994. Induction phenomena in gas hydrate nucleation. Chem. Eng. Sci. 49 (13), 2075–2087. https://doi.org/10.1016/0009-2509(94)E0026-M.

Nghiem, L., Yang, C., Shrivastava, V., Kohse, B., Hassam, M., Chen, D., Card, C., 2009. *Optimization of Residual Gas and Solubility Trapping for CO_2 Storage in Saline Aquifers* SPE Reservoir Simulation Symposium. https://doi.org/10.2118/119080-MS.

Nielsen, R.B., Bucklin, R.W., 1983. Why not use methanol for hydrate control. Hydrocarb. Process. 62 (4), 71–78.

Ochi, J., Vernoux, J.F., 1998. Permeability decrease in sandstone reservoirs by fluid injection: hydrodynamic and chemical effects. J. Hydrol. 208 (3), 237–248. https://doi.org/10.1016/S0022-1694(98)00169-3.

Ott, H., de Kloe, K., Marcelis, F., Makurat, A., 2011. Injection of supercritical CO_2 in brine saturated sandstone: pattern formation during salt precipitation. Energy Proc. 4, 4425–4432. https://doi.org/10.1016/j.egypro.2011.02.396.

Ott, H., Pentland, C.H., Oedai, S., 2015. CO_2–brine displacement in heterogeneous carbonates. Int. J. Greenh. Gas Control 33, 135–144. https://doi.org/10.1016/j.ijggc.2014.12.004.

Ott, H., Snippe, J., de Kloe, K., 2021. Salt precipitation due to supercritical gas injection: II. Capillary transport in multi porosity rocks. Int. J. Greenh. Gas Control 105, 103233. https://doi.org/10.1016/j.ijggc.2020.103233.

Pahlavanzadeh, H., Nouri, S., Aghajanloo, M., Mohammadi, A.H., Mohammadi, S., 2023. Experimental measurements and thermodynamic modeling of hydrate dissociation conditions for CO_2 + THF + $MgCl_2$ + water systems. Fluid Phase Equil. 564, 113626 https://doi.org/10.1016/j.fluid.2022.113626.

Pan, L., Lei, L., Seol, Y., 2021. Pore-scale influence of methane hydrate on permeability of porous media. J. Nat. Gas Sci. Eng. 87, 103758 https://doi.org/10.1016/j.jngse.2020.103758.

Pandey, J.S., Strand, O., von Solms, N., Almenningen, S., Ersland, G., 2022. Novel pore-scale visualization during CO_2 injection into CH_4 hydrate-saturated porous media. Energy & Fuels 36 (18), 10552–10571. https://doi.org/10.1021/acs.energyfuels.1c03878.

Pandey, J.S., Strand, Ø., von Solms, N., Ersland, G., Almenningen, S., 2021. Direct visualization of CH_4/CO_2 hydrate phase transitions in sandstone pores. Cryst. Growth Des. 21 (5), 2793–2806. https://doi.org/10.1021/acs.cgd.0c01714.

Parmesan, C., Morecroft, M.D., Trisurat, Y., 2022. *Climate Change 2022: Impacts, Adaptation and Vulnerability* GIEC.

Peter, A., Yang, D., Eshiet, K.I.-I., Sheng, Y., 2022. A review of the studies on CO_2 - brine - rock interaction in geological storage process. Geosciences 12 (4), 168. https://doi.org/10.3390/2076-3263/12/4/168.

Peters, D., Lacy, R., Dykhno, L., 2012. Flow Assurance in the Design and Operability of a CO_2 Transportation System. Offshore Technology Conference.

Pini, R., Krevor, S.C., Benson, S.M., 2012. Capillary pressure and heterogeneity for the CO_2/water system in sandstone rocks at reservoir conditions. Adv. Water Resour. 38, 48–59.

Priegnitz, M., Thaler, J., Spangenberg, E., Schicks, J.M., Schrötter, J., Abendroth, S., 2015. Characterizing electrical properties and permeability changes of hydrate bearing sediments using ERT data. Geophys. J. Int. 202 (3), 1599–1612.

Pruess, K., Müller, N., 2009. Formation dry-out from CO_2 injection into saline aquifers: 1. Effects of solids precipitation and their mitigation. Water Resour. Res. 45 (3).

Radhakrishnan, R., Trout, B.L., 2002. A new approach for studying nucleation phenomena using molecular simulations: application to CO_2 hydrate clathrates. J. Chem. Phys. 117 (4), 1786–1796. https://doi.org/10.1063/1.1485962.

Rehman, A.N., Bavoh, C.B., Pendyala, R., Lal, B., 2021. Research advances, maturation, and challenges of hydrate-based CO_2 sequestration in porous media. ACS Sustain. Chem. Eng. 9 (45), 15075–15108. https://doi.org/10.1021/acssuschemeng.1c05423.

Rempel, A., Buffett, B., 1997. Formation and accumulation of gas hydrate in porous media. J. Geophys. Res. Solid Earth 102 (B5), 10151–10164.

Rodger, P.M., 1990. Stability of gas hydrates. J. Phys. Chem. 94 (15), 6080–6089. https://doi.org/10.1021/j100378a082.

Roels, S.M., El Chatib, N., Nicolaides, C., Zitha, P.L., 2016. Capillary-driven transport of dissolved salt to the drying zone during CO_2 injection in homogeneous and layered porous media. Transport Porous Media 111 (2), 411–424.

Rossi, F., Gambelli, A.M., 2021. Thermodynamic phase equilibrium of single-guest hydrate and formation data of hydrate in presence of chemical additives: a review. Fluid Phase Equil. 536, 112958 https://doi.org/10.1016/j.fluid.2021.112958.

Rossi, F., Li, Y., Gambelli, A., 2021. Thermodynamic and kinetic description of the main effects related to the memory effect during carbon dioxide hydrates formation in a confined environment. Sustainability 13, 13797. https://doi.org/10.3390/su132413797.

Saadatpoor, E., Bryant, S.L., Sepehrnoori, K., 2010. New trapping mechanism in carbon sequestration. Transport Porous Media 82, 3–17.

Sahoo, S.K., Best, A.I., 2021. The influence of gas hydrate morphology on reservoir permeability and geophysical shear wave remote sensing. J. Geophys. Res. Solid Earth 126 (11), e2021JB022206.

Sayani, J.K.S., Pedapati, S.R., Lal, B., 2020. Phase behavior study on gas hydrates formation in gas dominant multiphase pipelines with crude oil and high CO_2 mixed gas. Sci. Rep. 10 (1), 14748 https://doi.org/10.1038/s41598-020-71509-6.

Semenov, A., Mendgaziev, R., Stoporev, A., Istomin, V., Tulegenov, T., Yarakhmedov, M., Novikov, A., Vinokurov, V., 2023. Direct measurement of the four-phase equilibrium coexistence vapor–aqueous solution–ice–gas hydrate in water–carbon dioxide system. Int. J. Mol. Sci. 24 (11), 9321. https://www.mdpi.com/1422-0067/24/11/9321.

Shagapov, V.S., Musakaev, N., Khasanov, M., 2015. Formation of gas hydrates in a porous medium during an injection of cold gas. Int. J. Heat Mass Tran. 84, 1030–1039.

Shen, S., Wang, L., Ge, Y., Chu, J., Liang, H., 2023. The effect of salinity on the strength behavior of hydrate-bearing sands. J. Mar. Sci. Eng. 11 (7), 1350. https://www.mdpi.com/2077-1312/11/7/1350.

Shotton, P., Vidal-Gilbert, S., Thibeau, S., Agenet, N., Lesueur, A., Manhes, C., Ninet, C., 2022. Aramis CO_2 Storage Case Study – A Geomechanical Assessment of Containment 16th Greenhouse Gas Control Technologies Conference. GHGT-16).

Singh, R.P., Shekhawat, K.S., Das, M.K., Muralidhar, K., 2020. Geological sequestration of CO_2 in a water-bearing reservoir in hydrate-forming conditions. Oil Gas Sci. Technol. – Rev. IFP Energies nouvelles 75, 51. https://doi.org/10.2516/ogst/2020038.

Sloan, E.D., 2003. Fundamental principles and applications of natural gas hydrates. Nature 426 (6964), 353–359. https://doi.org/10.1038/nature02135.

Sloan, E.D., Fleyfel, F., 1991. A molecular mechanism for gas hydrate nucleation from ice. AIChE J. 37, 1281–1292.

Sloan, E.D., Koh, C.A., 2008. Clathrate Hydrates of Natural Gases, third ed. CRC Press. https://doi.org/10.1201/9781420008494.

Smith, D.H., Wilder, J.W., Seshadri, K., 2002. Methane hydrate equilibria in silica gels with broad pore-size distributions. AIChE J. 48 (2), 393–400.

Snippe, J., Berg, S., Ganga, K., Brussee, N., Gdanski, R., 2020. Experimental and numerical investigation of wormholing during CO_2 storage and water alternating gas injection. Int. J. Greenh. Gas Control 94, 102901.

Sokama-Neuyam, Y.A., Yusof, M.A.M., Owusu, S.K., Darkwah-Owusu, V., Turkson, J.N., Otchere, A.S., Ursin, J.R., 2023. Experimental and theoretical investigation of the mechanisms of drying during CO_2 injection into saline reservoirs. Sci. Rep. 13 (1), 9155. https://doi.org/10.1038/s41598-023-36419-3.

Staykova, D.K., Kuhs, W.F., Salamatin, A.N., Hansen, T., 2003. Formation of porous gas hydrates from ice powders: diffraction experiments and multistage model. J. Phys. Chem. B 107 (37), 10299–10311. https://doi.org/10.1021/jp027787v.

Sum, A.K., Burruss, R.C., Sloan, E.D., 1997. Measurement of clathrate hydrates via Raman spectroscopy. J. Phys. Chem. B 101 (38), 7371–7377.

Sun, D., Englezos, P., 2016. CO_2 storage capacity in laboratory simulated depleted hydrocarbon reservoirs – impact of salinity and additives. J. Nat. Gas Sci. Eng. 35, 1416–1425. https://doi.org/10.1016/j.jngse.2016.03.043.

Talaghat, M.R., Khodaverdilo, A.R., 2019. Study of different models of prediction of the simple gas hydrates formation induction time and effect of different equations of state on them. Heat Mass Tran. 55 (5), 1245–1255. https://doi.org/10.1007/s00231-018-2508-y.

Talman, S., Shokri, A.R., Chalaturnyk, R., Nickel, E., 2020. Salt precipitation at an active CO_2 injection site. Gas injection into geological formations and related topics 183–199.

Tamáskovics, A., Kummer, N.-A., Amro, M., Alkan, H., 2023. Experimental investigation on the stability of gas hydrates under near-wellbore conditions during CO_2 injection for geologic carbon storage. Gas Science and Engineering 118, 205101. https://doi.org/10.1016/j.jgsce.2023.205101.

Torré, J.-P., Ricaurte, M., Dicharry, C., Broseta, D., 2012. CO_2 enclathration in the presence of water-soluble hydrate promoters: hydrate phase equilibria and kinetic studies in quiescent conditions. Chem. Eng. Sci. 82, 1–13. https://doi.org/10.1016/j.ces.2012.07.025.

Touil, A., Broseta, D., Desmedt, A., 2019. Gas hydrate crystallization in thin glass capillaries: roles of supercooling and wettability. Langmuir 35 (38), 12569–12581. https://doi.org/10.1021/acs.langmuir.9b01146.

Uchida, T., Ebinuma, T., Takeya, S., Nagao, J., Narita, H., 2002. Effects of pore sizes on dissociation temperatures and pressures of methane, carbon dioxide, and propane hydrates in porous media. J. Phys. Chem. B 106 (4), 820–826.

Vaessen, R., Van Der Ham, F., Witkamp, G., 2000. Eutectic freeze crystallization using CO_2 clathrates. Ann. N. Y. Acad. Sci. 912 (1), 483–495.

Valadbeygian, V., Hajipour, M., Behnood, M., 2023. Static and dynamic evaluation of formation damage due to barium sulfate scale during water injection in carbonate reservoirs. J. Pet. Explor. Prod. Technol. 13 (8), 1819–1831. https://doi.org/10.1007/s13202-023-01652-z.

Verma, A., Pruess, K., 1988. Thermohydrological conditions and silica redistribution near high-level nuclear wastes emplaced in saturated geological formations. J. Geophys. Res. Solid Earth 93 (B2), 1159–1173.

Vlasov, V.A., 2019. Mathematical model of the effect of self-preservation of gas hydrates. J. Eng. Phys. Thermophys. 92 (6), 1406–1414. https://doi.org/10.1007/s10891-019-02057-8.

Wang, L., Dou, M., Wang, Y., Xu, Y., Li, Y., Chen, Y., Li, L., 2022. A review of the effect of porous media on gas hydrate formation. ACS Omega 7 (38), 33666–33679. https://doi.org/10.1021/acsomega.2c03048.

Wang, P., Teng, Y., Zhao, Y., Zhu, J., 2021. Experimental studies on gas hydrate-based CO_2 storage: state-of-the-art and future research directions. Energy Technol. 9 (7), 2100004.

Wei, Y., Maeda, N., 2023. Mechanisms of the memory effect of clathrate hydrates. Chem. Eng. Sci. 270, 118538 https://doi.org/10.1016/j.ces.2023.118538.

Wells, J.D., Chen, W., Hartman, R.L., Koh, C.A., 2021. Carbon dioxide hydrate in a microfluidic device: phase boundary and crystallization kinetics measurements with micro-Raman spectroscopy. J. Chem. Phys. 154 (11).

Wen, Z., Yao, Y., Luo, W., Lei, X., 2021. Memory effect of CO_2-hydrate formation in porous media. Fuel 299, 120922. https://doi.org/10.1016/j.fuel.2021.120922.

White, M., 2011. Impact of Kinetics on the Injectivity of Liquid CO_2 into Arctic Hydrates. OTC Arctic Technology Conference.

Wroblewski, S., 1882. On the combination of carbonic acid and water. London, Edinburgh Dublin Phil. Mag. J. Sci. 13 (80), 228. https://doi.org/10.1080/14786448208627173. -228.

Wu, G., Tian, L., Ha, L., Feng, F., Yang, Z., Feng, J.C., Coulon, F., Jiang, Y., Zhang, R., 2022. Influence of pipeline steel surface on the thermal stability of methane hydrate. J. Mol. Liq. 367, 120486 https://doi.org/10.1016/j.molliq.2022.120486.

Wu, Y., Shang, L., Pan, Z., Xuan, Y., Baena-Moreno, F.M., Zhang, Z., 2021. Gas hydrate formation in the presence of mixed surfactants and alumina nanoparticles. J. Nat. Gas Sci. Eng. 94, 104049 https://doi.org/10.1016/j.jngse.2021.104049.

Xie, J., Delle Piane, C., Esteban, L., Brady, P.V., 2017. Fines migration during CO_2 injection: experimental results interpreted using surface forces. Int. J. Greenh. Gas Control 65, 32–39. https://doi.org/10.1016/j.ijggc.2017.08.011.

Xu, J., Bu, Z., Li, H., Wang, X., Liu, S., 2022. Permeability models of hydrate-bearing sediments: a comprehensive review with focus on normalized permeability. Energies 15 (13), 4524. https://www.mdpi.com/1996-1073/15/13/4524.

Xu, Q., Weir, G., Paterson, L., Black, I., Sharma, S., 2007. A CO_2-Rich Gas Well Test and Analyses. Asia Pacific Oil and Gas Conference and Exhibition.

Yagasaki, T., Matsumoto, M., Tanaka, H., 2015. Adsorption mechanism of inhibitor and guest molecules on the surface of gas hydrates. J. Am. Chem. Soc. 137 (37), 12079–12085. https://doi.org/10.1021/jacs.5b07417.

Yang, M., Dong, S., Zhao, J., Zheng, J.n., Liu, Z., Song, Y., 2021. Ice behaviors and heat transfer characteristics during the isothermal production process of methane hydrate reservoirs by depressurization. Energy 232, 121030. https://doi.org/10.1016/j.energy.2021.121030.

Yang, M., Song, Y., Liu, W., Zhao, J., Ruan, X., Jiang, L., Li, Q., 2013. Effects of additive mixtures (THF/SDS) on carbon dioxide hydrate formation and dissociation in porous media. Chem. Eng. Sci. 90, 69–76. https://doi.org/10.1016/j.ces.2012.11.026.

Yang, M., Song, Y., Liu, Y., Chen, Y., Li, Q., 2010. Influence of pore size, salinity and gas composition upon the hydrate formation conditions. Chin. J. Chem. Eng. 18 (2), 292–296. https://doi.org/10.1016/S1004-9541(08)60355-9.

Yang, M., Zhou, H., Wang, P., Song, Y., 2018. Effects of additives on continuous hydrate-based flue gas separation. Appl. Energy 221, 374–385. https://doi.org/10.1016/j.apenergy.2018.03.187.

Yang, S.H.B., Babu, P., Chua, S.F.S., Linga, P., 2016. Carbon dioxide hydrate kinetics in porous media with and without salts. Appl. Energy 162, 1131–1140.

Yin, Z., Moridis, G., Tan, H.K., Linga, P., 2018. Numerical analysis of experimental studies of methane hydrate formation in a sandy porous medium. Appl. Energy 220, 681–704. https://doi.org/10.1016/j.apenergy.2018.03.075.

Yin, Z., Zheng, J., Kim, H., Seo, Y., Linga, P., 2021. Hydrates for cold energy storage and transport: a review. Advances in Applied Energy 2, 100022. https://doi.org/10.1016/j.adapen.2021.100022.

You, K., Flemings, P.B., Malinverno, A., Collett, T.S., Darnell, K., 2019. Mechanisms of methane hydrate formation in geological systems. Rev. Geophys. 57 (4), 1146–1196. https://doi.org/10.1029/2018RG000638.

Yusof, M.A.M., Neuyam, Y.A.S., Ibrahim, M.A., Saaid, I.M., Idris, A.K., Mohamed, M.A., 2022. Experimental study of CO_2 injectivity impairment in sandstone due to salt precipitation and fines migration. J. Pet. Explor. Prod. Technol. 12 (8), 2191–2202. https://doi.org/10.1007/s13202-022-01453-w.

Zatsepina, O.Y., Buffett, B.A., 2002. Nucleation of CO_2-hydrate in a porous medium. Fluid Phase Equil. 200 (2), 263–275. https://doi.org/10.1016/S0378-3812(02)00032-8.

Zha, L., Liang, D.Q., Li, D.L., 2012. Phase equilibria of CO_2 hydrate in NaCl–$MgCl_2$ aqueous solutions. J. Chem. Therm. 55, 110–114. https://doi.org/10.1016/j.jct.2012.06.025.

Zhang, G., Liu, B., Xu, L., Zhang, R., He, Y., Wang, F., 2021. How porous surfaces influence the nucleation and growth of methane hydrates. Fuel 291, 120142. https://doi.org/10.1016/j.fuel.2021.120142.

Zhang, P., Wu, Q., Mu, C., Chen, X., 2018. Nucleation mechanisms of CO_2 hydrate reflected by gas solubility. Sci. Rep. 8 (1), 10441 https://doi.org/10.1038/s41598-018-28555-y.

Zhang, S., Liu, H.H., 2016. Porosity–permeability relationships in modeling salt precipitation during CO_2 sequestration: review of conceptual models and implementation in numerical simulations. Int. J. Greenh. Gas Control 52, 24–31. https://doi.org/10.1016/j.ijggc.2016.06.013.

Zhang, Z., Guo, G.J., 2017. The effects of ice on methane hydrate nucleation: a microcanonical molecular dynamics study [10.1039/C7CP03649C]. Phys. Chem. Chem. Phys. 19 (29), 19496–19505. https://doi.org/10.1039/C7CP03649C.

Zhao, J., Fan, Z., Dong, H., Yang, Z., Song, Y., 2016. Influence of reservoir permeability on methane hydrate dissociation by depressurization. Int. J. Heat Mass Tran. 103, 265–276.

Zhao, J., Tian, Y., Zhao, Y., Cheng, W., 2015a. Experimental investigation of effect on hydrate formation in spray reactor. J. Chem. 2015.

Zhao, J., Yang, L., Liu, Y., Song, Y., 2015b. Microstructural characteristics of natural gas hydrates hosted in various sand sediments [10.1039/C5CP03698D]. Phys. Chem. Chem. Phys. 17 (35), 22632–22641. https://doi.org/10.1039/C5CP03698D.

Zhao, Q., Chen, Z.-Y., Li, X.-S., Xia, Z.-M., 2023. Experimental study of CO_2 hydrate formation under an electrostatic field. Energy 272, 127119. https://doi.org/10.1016/j.energy.2023.127119.

Zheng, J.n., Yang, M., Chen, B., Song, Y., Wang, D., 2017. Research on the CO_2 gas uptake of different hydrate structures with cyclopentane or methyl-cyclopentane as Co-guest molecules. Energy Proc. 105, 4133–4139. https://doi.org/10.1016/j.egypro.2017.03.877.

Zheng, J., Chong, Z.R., Qureshi, M.F., Linga, P., 2020. Carbon dioxide sequestration via gas hydrates: a potential pathway toward decarbonization. Energy & Fuels 34 (9), 10529–10546. https://doi.org/10.1021/acs.energyfuels.0c02309.

Ziabakhsh-Ganji, Z., Kooi, H., 2014. Sensitivity of Joule–Thomson cooling to impure CO_2 injection in depleted gas reservoirs. Appl. Energy 113, 434–451. https://doi.org/10.1016/j.apenergy.2013.07.059.

Zuniga, A.R., 2020. NMR Studies of Natural Gas Hydrates Exposed to Thermally Controlled CO_2 Exchange. The University of Western Australia.

Zuo, Y.-X., Stenby, E.H., 1997. Prediction of gas hydrate formation conditions in aqueous solutions of single and mixed electrolytes. SPE J. 2 (4), 406–416. https://doi.org/10.2118/31048-pa.